Nonlinear Raman Studies of Weakly Bound Complexes and Clusters in Molecular Beams

Peter M. Felker,* Patrick M. Maxton, and Mark W. Schaeffer

Department of Chemistry and Biochemistry, University of California, Los Angeles, California 90024-1569

Received February 9, 1994 (Revised Manuscript Received May 9, 1994)

Contents

I. Introduction

In the past decade, largely because of advances in the vibrational spectroscopic study of species in cold molecular beams, significant progress has been made in elucidating the ground-state properties of weakly bound complexes and clusters. (For reviews see refs 1–4). Indeed, vibrational results have been essential to the deduction of that most central of properties in van der Waals molecule studies—the intermolecular potential energy surface.

Thus far, most ground-state (ro)vibrational studies of van der Waals species have relied on spectroscopic methods in the infrared (both mid- and far-IR) spectral region.[1-4] A substantial number of other studies have employed stimulated emission (e.g., refs 5–8) and/or dispersed fluorescence spectroscopies (e.g., refs 9 and 10). Until fairly recently, however, the use of *Raman-based* techniques for van der Waals molecule studies had been quite limited. The inherent weakness of the Raman effect and the general sparseness of seeded molecular-beam samples effectively preclude the use of spontaneous Raman methods in almost all such studies. On the other hand, it has now been amply demonstrated[11,12] that nonlinear Raman spectroscopies do have the sensitivity to be valuable in experiments on jet-cooled van der Waals species. This is a significant development given that results from Raman-based experiments provide information that often cannot be obtained from other spectroscopic methods (because of selection rules or propensity rules). Moreover, nonlinear Raman methods can easily be implemented at subwavenumber resolution throughout the entire vibrational fundamental region. They can readily serve as the basis for time-domain (pump–probe) experiments aimed at studying dynamical processes. And, some of these methods are characterized by very high sensitivity, as well as by excellent size- and species-selectivity. It is not unreasonable to project that Raman-based experiments will become increasingly important sources of information on the properties of weakly bound species.

This paper reviews applications of nonlinear Raman spectroscopies to the study of van der Waals complexes and clusters in cold, supersonic molecular beams. The review is limited to those studies that have employed Raman schemes unenhanced by vibronic resonance. Thus, we do not include consideration of the various stimulated emission spectroscopies[5-8] or resonantly enhanced coherent Raman methods.[13,14] The organization of the paper is as follows. In section II the relevant spectroscopic schemes along with their strengths and weaknesses are outlined. Section III pertains to results on small homogeneous complexes and clusters. Section IV deals with results on heterogeneous complexes. In section V, the results on larger homogeneous clusters are outlined. Section VI then deals with results on heterogeneous clusters. Finally, section VII is a summary and conclusion.

II. Experimental Methods

There are three types of nonlinear Raman spectroscopies that have thus far been employed in studies of weakly bound species—coherent Raman scattering (CRS),[11] stimulated Raman loss (SRL) or gain (SRG),[11] and mass-selective, ionization-detected stimulated Raman spectroscopies (IDSRS).[12] We consider each of these with a focus on those characteristics that are particularly relevant to molecular-beam studies. We also briefly consider the Fourier-

0009-2665/94/0794-1787$14.00/0 © 1994 American Chemical Society

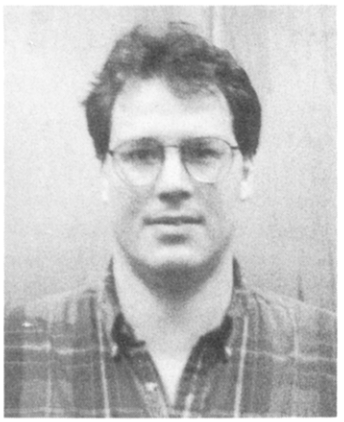

Peter M. Felker was born in Rochester, NY. He received his B.S. in Chemistry (1979) from Union College in Schenectady, NY, and his Ph.D. in Chemical Physics (1984) from the California Institute of Technology, under the direction of Professor A. H. Zewail. After a year as a postdoctoral fellow at CalTech he joined the Department of Chemistry and Biochemistry at UCLA, where he is now a Professor of Chemical Physics. His research interests pertain to the development of ultrafast and nonlinear spectroscopies and their application in studies of molecular dynamics, structure, and intermolecular interactions. He has received an NSF Presidential Young Investigator Award, an Alfred P. Sloan Fellowship, and the Coblentz Award from the Coblentz Society.

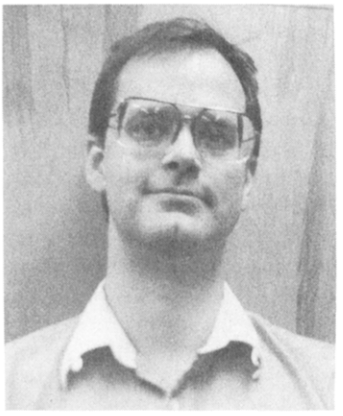

Patrick M. Maxton was born in 1957 in Wichita, KS. He received a B.S. degree in physics from Wichita State University (1979), a M.A. from University of California, Berkeley (1981), and a Ph.D. from UCLA. He is currently a postdoctoral scholar at UCLA. His research interests include nonlinear dynamics and nonlinear laser spectroscopy.

transform implementations of the nonlinear Raman schemes,[12,15] some of which have proved useful in studies of weakly bound complexes and clusters.

A. Coherent Raman Scattering

The earliest applications of nonlinear Raman techniques in molecular-beam spectroscopy[16,17] involved the use of coherent Raman scattering (CRS),[11] and CRS remains very powerful in studies of jet-cooled complexes and clusters. Figure 1a shows a level diagram relating to the processes involved in the anti-Stokes version of CRS. A stimulated Raman process driven by the ω_1 and ω_2 fields creates a material coherence in the sample. A third field (ω_3) then interacts with that coherence to produce a highly directional signal beam at frequency $\omega_1 + \omega_3 - \omega_2$. The signal beam is isolated by spatial, spectral, and/or polarization filtering, and its intensity as a function of $\omega_1 - \omega_2$ gives the Raman spectrum of the sample.

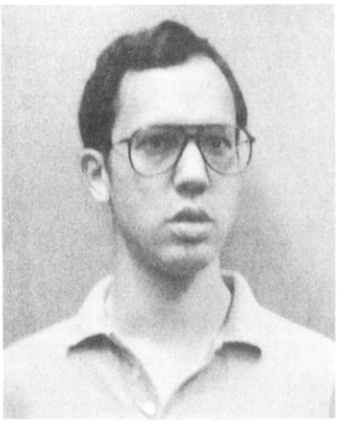

Mark W. Schaeffer was born in Rochester, NY, in 1960. He earned a B.S. in Computer Engineering from the University of California, San Diego, in 1982, and a M.S. in Electrical and Computer Engineering from the University of California, Santa Barbara, in 1989. From 1982 to 1989 he worked for the U.S. Navy at Pacific Missile Test Center, Point Mugu, CA, as an electronics engineer. He earned a B.S. in Chemistry at the University of California, Irvine, in 1991, working in F. Sherwood Rowland's atmospheric chemistry laboratory. He then entered the University of California, Los Angeles, where he is a doctoral candidate in Physical Chemistry working in the laboratory of Peter M. Felker. He is a recipient of the UCLA University Fellowship (1991–1995). His research interests include ionization-detected stimulated Raman spectroscopy of molecular clusters.

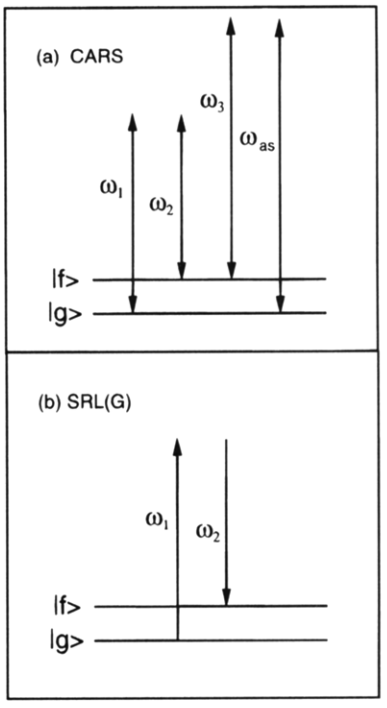

Figure 1. (a) Level diagram depicting processes involved in coherent anti-Stokes stimulated Raman scattering. The ω_1, ω_2, and ω_3 fields all arise from lasers. The ω_{as} field is the signal in the experiment. It has appreciable intensity when $\omega_1 - \omega_2$ is resonant with the $|f\rangle \leftarrow |g\rangle$ transition. Part b is a level diagram depicting the process involved in SRL and SRG. In both cases the ω_1 and ω_2 fields drive a stimulated Raman transition. In SRL the intensity of the ω_1 field is monitored, and a loss in its intensity signals the efficient driving of a stimulated Raman resonance. In SRG the intensity of the ω_2 field is monitored, and a gain in its intensity reflects the efficient driving of a stimulated Raman resonance.

CRS has several desirable features in cluster studies. First, it is largely a zero-background method, in principle. Second, with appropriate focusing ge-

ometries at the sample,[18] it can be used to measure Raman spectra down to 0 cm^{-1}. Hence, it is valuable in characterizing the low-frequency collective motions in clusters.[11,19,20] Third, since CRS signal is typically generated from rather small focal volumes, the method can be used as a spatially selective probe of how cluster properties evolve during the course of a supersonic expansion.[19] Fourth, there are, in principle, no limitations with regard to that portion of the molecular beam expansion that can be probed by CRS. (For example, there is no need to have a skimmed beam, as in mass-selective IDSRS methods.) In practice, though, the scaling of CRS intensity with sample density (see below) places limits on how far away from the expansion orifice one can go and still obtain useful signal levels. Fifth, all molecular species can give rise to coherent Raman scattering. Species that are inaccessible to infrared, stimulated emission, fluorescence, or resonance-enhanced photoionization-based spectroscopies can be studied with CRS.

The disadvantages of CRS in studies of weakly bound species are as follows. First, its sensitivity is not as high as methods based on fluorescence or photoionization detection. A large part of this reduction in sensitivity is due to the scaling of CRS intensity with the *square* of the density of relevant species in the sample.[11] For sparse molecular beam samples this quadratic scaling can have a very detrimental effect on signal levels. A further reduction in sensitivity can arise if appreciable nonresonance CRS signals[11] are produced in the sample (from the carrier gas, for example). This latter effect is not as pernicious as it is in condensed-phase systems, however. Second, CRS is not markedly size- or species-selective. (Vibronic-resonance-enhanced versions[13] can be, however.) One must rely on spectral resolution and/or must try to produce a narrow distribution of cluster types in the sample in order to obtain some measure of selectivity. For this reason, and for reasons of sensitivity, CRS is perhaps most powerful in application to large, homogeneous clusters. Third, a CRS spectrum is essentially the square of a spontaneous Raman spectrum. This has the effect of enhancing the strongest features at the expense of the weaker ones.

B. Stimulated Raman Loss (Gain)

In stimulated Raman loss and gain spectroscopies,[11,21] stimulated Raman transitions induced by the ω_1 and ω_2 fields of Figure 1b are detected by monitoring the intensity of one of those fields. When $\omega_1 - \omega_2$ is on a Raman resonance ω_1 photons are consumed and ω_2 photons are created. Hence, a stimulated Raman loss experiment entails detecting the loss in ω_1 intensity as a function of $\omega_1 - \omega_2$, while stimulated Raman gain entails detecting the gain in ω_2 intensity as a function of $\omega_1 - \omega_2$.

The desirable and undesirable characteristics of SRL(G) in regard to cluster studies are quite similar to those of CRS. One significant difference, however, is that signal levels in SRL(G) scale linearly with sample density and with Raman strength, as opposed to quadratically. As a consequence, one does not pay the heavy price in sensitivity that one does with CRS when studying sparser samples, sparser regions of a given sample (e.g., see ref 22), or weaker Raman transitions. A second difference is that there is no phase-matching requirement in SRL(G) as there is in CRS. Thus, any convenient excitation-field geometry can be employed in the former. Finally, nonresonant Raman processes do not have the pernicious effects in SRL(G) that they can have in CRS.

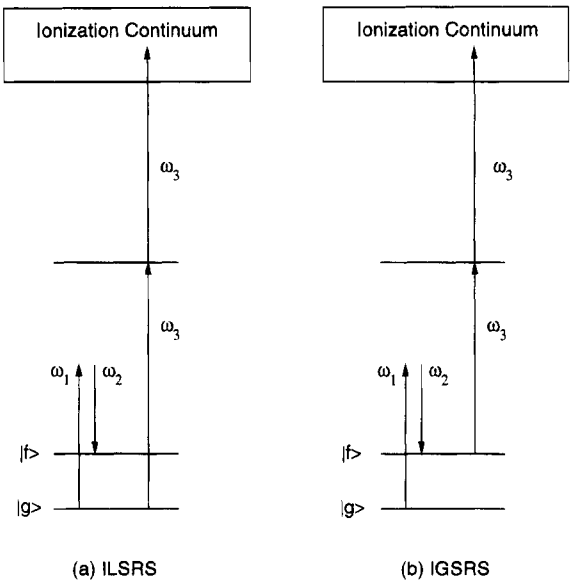

Figure 2. (a) Level diagram depicting the processes involved in ionization-loss stimulated Raman spectroscopy. ω_1 and ω_2 drive a stimulated Raman transition. ω_3 probes, by resonantly enhanced multiphoton ionization (REMPI), the loss in the $|g\rangle$-state population due to such transitions. Part b is a level diagram depicting the processes involved in ionization-gain stimulated Raman spectroscopy. In this case the ω_3 field monitors (by REMPI) the gain in $|f\rangle$-state population due to stimulated Raman transitions.

C. Mass-Selective, Ionization-Detected Stimulated Raman Spectroscopies

Ionization-detected stimulated Raman spectroscopies employ resonantly enhanced multiphoton ionization (REMPI) to probe the population changes induced by stimulated Raman transitions. In ionization-loss stimulated Raman spectroscopy[23] (ILSRS) (Figure 2a) a two-color light pulse (ω_1,ω_2) drives a stimulated Raman transition $|f\rangle \leftarrow |g\rangle$. A second light pulse ($\omega_3$), delayed from the first, is tuned such that it photoionizes by REMPI those species that remain in state $|g\rangle$. Raman resonances are thus registered as a loss in baseline photoion signal as $\omega_1 - \omega_2$ is tuned. In ionization-gain stimulated Raman spectroscopy[24,25] (IGSRS) the scheme is the same (Figure 2b) except that the REMPI pulse is tuned to a vibronic transition originating in $|f\rangle$. In this case, a stimulated Raman resonance is registered as a gain in photoion signal as $\omega_1 - \omega_2$ is tuned. Finally, in IGSRS "probe spectroscopy" $\omega_1 - \omega_2$ is fixed to a known Raman resonance and REMPI signal is then monitored as ω_3 is scanned.[24,25] In this manner, the vibronic spectrum originating in $|f\rangle$ can be measured. All three of these schemes can be readily implemented with mass-selective detection of the photoions produced.[12] Indeed, such mass analysis is central to the usefulness of IDSRS methods in studies of van der Waals species.

The strengths of mass-selective IDSRS methods in cluster studies are severalfold.[12] First, the techniques are very sensitive. This comes from the high sensitivity of the REMPI probe scheme and from the ability to effect large fractional population transfers by means of stimulated Raman transitions. Second, they can be very size-selective and, indeed, species-selective. Mass-selective detection is a principal reason for such selectivity. In addition, the vibronic resonance requirement, coupled with the fact that different cluster isomers often have resolvably different vibronic spectra, allows for a significant degree of species selectivity. Third, the double-resonance nature of IDSRS schemes allows for the correlation of vibrational and vibronic resonances. Fourth, even though an accessible vibronic chromophore must be present if a species is to be studied by IDSRS, Raman resonances need not be localized in that vibronic chromophore to be observable. This is because Raman-dependent cluster-fragmentation channels can produce depletions in mass-selective ILSRS even when the Raman excitation does not significantly perturb the vibronic chromophore. Finally, like all nonlinear Raman schemes, the IDSRS methods permit wide spectral coverage at subwavenumber resolution with a single laser system.

The limitations of IDSRS methods are as follows. First, the methods are applicable only to species with accessible vibronic chromophores. Second, the mass-selective variants require a skimmed molecular beam and a differentially pumped laser interaction region. Thus, one cannot do mass-selective IDSRS experiments at small distances from the molecular-beam expansion orifice, as can be done with CRS or SRL-(G). Third, IDSRS spectra are stimulated Raman action spectra. They are stimulated Raman spectra convoluted with the REMPI probe process. Hence, they are not always simple replications of species' Raman spectra. Fourth, IGSRS signals are subject to decay processes originating in the Raman-excited state. Decay processes occurring on time scales faster than the laser pulsewidths can preclude the observation of IGSRS signals. This is one reason why all the IDSRS results on clusters larger than trimers have been obtained by mass-selective ILSRS.

D. Fourier-Transform Nonlinear Raman Spectroscopies

Raman spectral resolution in the methods described above depends on the bandwidths of the ω_1 and ω_2 light sources. High resolution requires narrow bandwidths for both sources. On the other hand, the high intensities required to drive stimulated Raman processes efficiently is a factor that works against the ready production of very narrow bandwidths. One way to get around this is to employ interferometric, Fourier-transform versions of the nonlinear Raman spectroscopies.[12,15,26,27] In these schemes the ω_1 and ω_2 stimulated Raman fields are sent through a Michelson interferometer such that they both experience the same optical delay. The output of the interferometer is combined with any probe fields required, and the signal appropriate to the particular spectroscopic method employed is monitored as a function of interferometer delay. The result is an interferogram that is modulated at the frequencies of those Raman resonances driven by the ω_1, ω_2 fields. The Fourier transform of such an interferogram yields the pertinent nonlinear Raman spectrum of the sample at a spectral resolution that does not depend on the light-source bandwidths, but that does depend on the interferometer delay range encompassed by the interferogram. The point is that high spectral resolution is available, in principle, even when the ω_1, ω_2 light sources have broad bandwidths. Fourier-transform versions of CRS[26] and IDSRS[12,26] (as well as stimulated emission[27] and hole-burning[27] spectroscopies) have been demonstrated. The FT-IDSRS schemes have been employed in experiments on dimers[28] and trimers,[29] as well as on bare molecules. Some of these results are discussed below.

III. Homogeneous Dimers

A. CO_2 Dimer

One of the first applications of nonlinear Raman methods to a van der Waals (vdW) molecule was a coherent anti-Stokes Raman spectroscopic (CARS) study of CO_2 dimer by Pubanz et al.[30] The study was primarily concerned with shedding light on the geometry of the species. Prior work involving electric deflection,[31,32] gas-phase[33-36] and matrix-isolation infrared spectroscopy,[37,38] and theoretical calculations[39-41] had come to no consensus on this issue. Both a polar, T-shaped structure and a nonpolar parallel-displaced structure had been proposed on the basis of the various results. The CARS experiments pertained to the lower member of the $2\nu_2-\nu_1$ Fermi dyad region of CO_2 near 1285 cm^{-1}. Spectra were measured at 0.3 and 0.05 cm^{-1} resolution on molecular beams of CO_2 seeded in He. Four bands were observed to the red of the monomer CO_2 Q branch at 1285.5 cm^{-1}, and these were attributed to complexes and clusters. On the basis of the pressure and nozzle-temperature dependence of intensities, the least red-shifted of the bands at 1281.3 cm^{-1} was assigned to CO_2 dimer. The others were assigned to higher clusters. Comparison of the CARS data on the dimer with previous infrared results[34] revealed that the two dimer bands correlating with the lower Fermi dyad member obey the rule of mutual exclusion—that is, one is only infrared active and the other is only Raman active. On this basis it was argued that the structure of the dimer was most likely the displaced parallel geometry rather than the T-shape; the latter would be expected to have two ν_1 fundamentals of similar intensity in both the Raman and infrared spectra. Subsequent high-resolution, bolometer-detected infrared experiments on the $\nu_1 + \nu_3$ combination band of the dimer[42] unambiguously substantiated the conclusions made on the basis of the CARS spectra.

B. HCN Complexes

A second very early application of nonlinear Raman spectroscopy to the study of weakly bound species involved CARS spectroscopy of jet-cooled HCN complexes, experiments which were carried out in conjunction with FTIR and photoacoustic nonlinear Raman experiments (PARS) on such species in a low-

temperature, static-gas sample.[43,44] Due to the particular focus of this review we concentrate on the molecular-beam CARS results here. CARS results were obtained at 0.3 and 0.05 cm^{-1} resolution in the CN stretch and CH stretch regions of HCN and DCN aggregates formed in neat and seeded (in Ar and He) expansions. Bands were observed that were assigned to HCN dimer, trimer, and higher polymers. Marked changes in the degree of aggregation, as manifested in the CARS spectra, were found as expansion conditions changed. The results were primarily used in helping to refine harmonic force fields for the dimer and trimer. In this regard, the ability of nonlinear Raman methods to access vibrational resonances difficult or impossible to access by other means was put to good advantage. Also notable is the overlap of spectral features assigned to HCN (DCN) polymers with the analogous vibrational bands in bulk, crystalline HCN. This was taken as evidence that intermolecular interactions in the clusters and in the crystal (as opposed to the liquid) are similar. Perhaps the major value of this early work, however, was in clearly demonstrating the potential of nonlinear Raman methods in application to weakly bound, jet-cooled species.

In a later set of high-resolution infrared studies of HCN complexes, Jucks and Miller[45,46] presented results for the CH stretch region that supersede some of the results of refs 43 and 44. In particular, they reported the observation of both dimer CH stretch fundamentals, all three CH stretch fundamentals of the linear trimer, the single IR-active CH stretch fundamental of the cyclic trimer, and higher-cluster (probably tetramer) CH stretch bands. One of the dimer bands reported in ref 45 coincides with a CARS band attributed to the dimer. However, the IR trimer bands are all at significantly higher frequencies than the feature attributed to trimers in ref 44. In the light of the IR results, it is clear that the major feature observed in the CH stretch region of the CARS spectra is due solely to larger clusters of HCN.

C. Benzene Dimer

1. Intramolecular Raman Transitions

Henson et al.[28,47,48] have made an extensive study of benzene dimer and isotopomers thereof by applying mass-selective IDSRS methods to the characterization of "intramolecular" vibrations in the species. In particular, dimer bands correlating with the ν_1 (totally symmetric ring-breathing mode) and ν_2 (totally symmetric CH stretch) fundamentals were studied. Less extensive results were also obtained on the ν_6 fundamentals of the dimers. The earliest experiments related to vibrational dynamics.[48] Mass-selective IGSRS experiments were performed in the ν_1 region near 993 cm^{-1}, with the REMPI probe pulse tuned to the $1_1^0 6_0^1$ vibronic band of the species and delayed by greater than 10 ns from the Raman pump pulse. Despite such a delay, IGSRS signal could nevertheless be observed. The data therefore clearly showed that the ν_1-excited dimer lives for nanoseconds or longer. Subsequent pump−probe IGSRS experiments gave a lifetime of 30−40 ns for the fully protonated isotopomer.[28] This lifetime is much longer than one might have expected given the many low-frequency van der Waals modes in the dimer and the resulting large density of vibrational states at 993 cm^{-1}. It is also much longer than would have been expected in the light of infrared predissociation studies[49] of the species at 1038 cm^{-1}, from which lifetimes of just a few picoseconds were derived from line-width data.

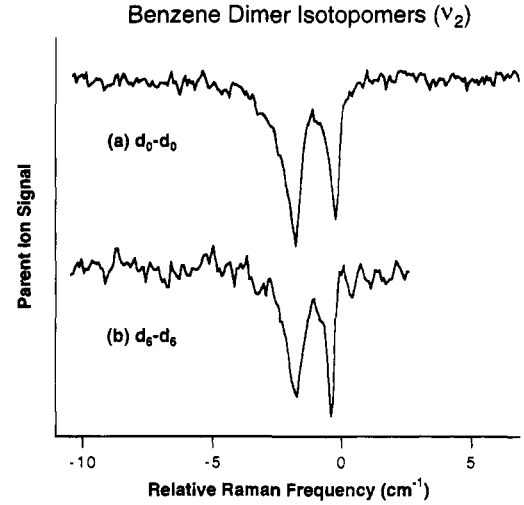

Figure 3. Mass-selective ILSRS spectra of benzene dimer isotopomers: (a) spectrum of the fully protonated dimer in the region of the ν_2 fundamental of benzene near 3074 cm^{-1} and (b) spectrum of the fully deuterated dimer in the region of the ν_2 fundamental of benzene-d_6 near 2303 cm^{-1}. The zero of the frequency scale in both spectra corresponds to the frequency of the relevant monomer ν_2 fundamental. For further details see ref 28.

The bulk of Henson et al.'s mass-selective IDSRS work on benzene dimer has been directed toward characterization of the species' geometry,[28,47] a topic of considerable earlier work that had not led to a definitive conclusion. Several results bearing on this issue were obtained. First, for both the fully protonated and the fully deuterated dimer two ν_1 and two ν_2 fundamentals are present. Moreover, in all the mixed isotopomers studied there are two ν_1 and two ν_2 fundamentals per monomer moiety. Figures 3 and 4 show spectra relevant to these points. Such behavior is proof that the dimer is composed of benzenes residing in *inequivalent* sites. This conclusion is further supported by (1) the pattern of splittings and shifts observed for the Raman bands, (2) the results of IGSRS probe spectroscopy, and (3) double-resonance results proving the presence of two isomeric forms for each mixed isotopomer. With regard to the first point, the positions of the observed ν_1 and ν_2 bands could be readily rationalized by assuming inequivalent benzene moieties and by accounting for the effects of site shifts and excitation-exchange interactions. In doing this, consistent values for the site shifts and excitation-exchange interactions were found for all of the isotopomers studied. With regard to the second point, the IGSRS probe spectroscopy pertaining to the ν_1 Raman bands revealed markedly different vibronic structure depending on which ν_1 band was excited. Examples of such spectra are shown in Figure 4b. Clearly, this is consistent with vibronic excitations localized in benzene moieties that reside in significantly different environments. Finally, with regard to the third point, a dimer geometry composed of inequivalent benzenes would be expected to give rise to two

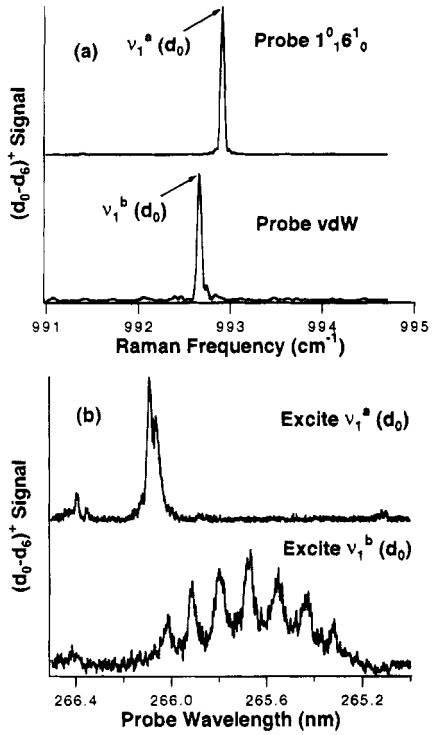

Figure 4. (a, top) Fourier transform IGSRS spectrum (0.05 cm^{-1} resolution) in the region of the h_6-benzene-localized ν_1 fundamental of the d_0–d_6 benzene dimer isotopomer. The spectrum was measured with ω_3 set to the d_0-localized $1^0_1 6^1_0$ band of the heterodimer. The bottom spectrum is the same except that ω_3 was set to the second van der Waals band built off of the h_6-localized $1^0_1 6^1_0$ vibronic band. (b, top) IGSRS probe spectrum of the d_0–d_6 heteroisotopomer taken subsequent to excitation of the Raman band in the spectrum of a, top. (Bottom) IGSRS probe spectrum of the d_0–d_6 heteroisotopomer taken subsequent to excitation of the Raman band in the spectrum of a, bottom. For further details, see ref 28.

isomers for each isotopically mixed dimer by virtue of the possibility for interchange of isotopically distinct monomers between the two inequivalent sites. Such would not be expected if the sites were equivalent.

A second issue addressed by the mass-selective IDSRS results[28] pertains to the symmetries of the two inequivalent sites in benzene dimer. In principle, each heteroisotopomer of the dimer should produce *four* different $S_1 \leftarrow S_0$ 0^0_0 bands, assuming inequivalent sites for the monomer moieties. This is because each heteroisotopomer should have two isomers (see above) and each isomer should have 0^0_0 bands localized in each of its two benzene moieties. Despite this, however, only two 0^0_0 bands per heteroisotopomer have been observed. Henson et al. proposed one site in the dimer to be of high symmetry and the other to be of lower symmetry to account for this behavior. This interpretation is based on the fact that the $S_1 \leftarrow S_0$ 0^0_0 bands of benzene are only dipole-allowed when the molecule is in an environment of less than C_{3v} symmetry. The interpretation implies that the two 0^0_0 bands observed for the d_0–d_6 heteroisotopomer are, in fact, due to the two distinct isomers of this species. That is, one of the bands corresponds to a d_0-localized excitation in the isomer for which the d_0 monomer moiety is in the low-symmetry site. The other band corresponds to a d_6-localized excitation in the isomer for which the d_6 monomer resides in the low-symmetry site. By using the mass-selective ILSRS technique with ω_3 tuned to one or the other of the 0^0_0 bands for the d_0–d_6 isotopomer, Henson et al.[28] were able to correlate the shifts of Raman bands with the particular vibronic band being probed. Such correlation clearly showed that the observed 0^0_0 bands are associated with the same site in the dimer, as expected. In short, the IDSRS evidence lends strong support to one site of high and one of low symmetry in benzene dimer.

Finally, to account for all the IDSRS results Henson et al.[28] proposed a T-shaped dimer geometry involving free, or near-free, internal rotation about the axis connecting the mass centers of the monomer moieties. The T-shape geometry had been predicted to be the lowest-energy form by *ab initio* electronic-structure calculations.[50] It is that which characterizes the nearest-neighbor interactions in benzene crystal.[51] And, it had been proposed in prior dimer studies to account for a nonzero dimer dipole moment[52] and for the close match between the splitting of the $S_1 \leftarrow S_0$ 6^1_0 band in the dimer and in the crystal.[53] The T-shaped dimer with internal rotation has inequivalent sites with one (the stem) being of low symmetry and the other (the top) being of high effective symmetry because of the averaging from internal rotation. Hence, the structure does account for the major conclusions taken from the IDSRS results. Moreover, it was also found to be consistent with other important aspects of the IDSRS data. In particular, Henson et al. could readily rationalize the pattern of Raman bandshifts, the markedly different vibronic spectra associated with the benzenes in the two sites (see Figure 4b), and the significantly different widths of the ν_2 Raman bands associated with the different sites (see Figure 3), in terms of the T-shape geometry.

Besides the work of Henson et al., Ito et al.[54] have also reported mass-selective IDSRS results on benzene dimer. One important aspect of their work is the measurement of the Raman polarization ratios for the two ν_1 bands present in the fully protonated dimer. They observed significantly different ratios for these bands and suggested that the behavior might be due to two different dimer isomers. However, this interpretation is not consistent with the results of ref 28, which clearly show the two relevant Raman bands to be due to the same species. In fact, the different polarization ratios of the two bands can be rationalized in another way by considering how the isotropic and anisotropic polarizability components associated with the two ν_1 fundamentals in the dimer are modified by excitation-exchange coupling. One can show that the higher-frequency ν_1 band has its anisotropic part enhanced relative to its isotropic part, whereas the opposite obtains for the lower-frequency band. Hence, the measured polarization ratios are indeed consistent with the results of ref 28.

Finally, experiments other than ones based on nonlinear Raman methods have recently been reported that bear on the benzene dimer Raman results. Scherzer et al.[55] have used vibronic hole-burning spectroscopy to confirm that the dimer is

composed of inequivalent benzene moieties. Arunan and Gutowsky[56] have been successful in resolving rotational structure of the dimer by pulsed, Fourier-transform microwave spectroscopy. Their results appear to be consistent with Henson et al.'s proposal of a T shape with internal rotation, although a full analysis of the rotational results has not yet been reported. Finally, experimental[55] and theoretical[57] results point to the existence of stable dimer conformers different than the one that is the spectroscopically dominant one. It is likely that mass-selective IDSRS experiments will prove very valuable in characterizing these other benzene dimer species.

2. Intermolecular Raman Transitions

Venturo and Felker[58] have reported the application of mass-selective IDSRS to the study of intermolecular vibrational transitions in benzene dimer isotopomers. For each of four dimer species three bands were observed with 0.3 cm^{-1} resolution by mass-selective ILSRS, one at about 3.5 cm^{-1}, a second at 9−10 cm^{-1}, and a third at 47−53 cm^{-1}. All of these bands were found to be absent a ^qQ branch and to exhibit much greater rotational broadening than the intramolecular Raman bands of the dimer. The 9−10 cm^{-1} band was observed to be very strongly Raman active, producing depletions of greater than 20%, despite the presence of a rotational width significantly larger than the Raman resolution. IGSRS signals were also observed for the 9−10 cm^{-1} band when the REMPI probe frequency was tuned a few cm^{-1} to the red of the 0_0^0 or 6_0^1 vibronic bands. In this way the ground-state Raman interval could be correlated with a smaller intermolecular vibrational interval in the S_1 manifold. Finally, the 9−10 cm^{-1} band was found to have an isotopic shift pattern in which perdeuteration of the benzene moiety in the high-symmetry dimer site (the top of the T, assuming a T-shaped structure) produces a red shift significantly less than that arising from perdeuteration at the low-symmetry site (stem of the T). Preliminary results suggested that just the opposite isotopic shift pattern obtains for the band in the 47−53 cm^{-1} region.

On the basis of the IDSRS results and other information on the dimer, preliminary assignments of the intermolecular bands were made. All were assigned to internal−rotational or librational motions of the benzene moieties. Such motions, because of the large permanent polarizability anisotropy of benzene,[59] would be expected to be strongly Raman active (see section IV.B.2). They would also be expected to impart their Raman activity by modulating the anisotropic part of the dimer's polarizability tensor and, hence, to produce broad rotational band contours without ^qQ branches, as observed. The lowest frequency band was attributed to transitions between internal rotational levels based on the other strong evidence for such a motion[28,56] and on the expectation that its frequency would be very low. On the basis of its isotopic shifts, the 9−10 cm^{-1} band was attributed to a librational mode primarily involving hindered rotation of the benzene in the stem-of-the-T site about one of its in-plane axes. Finally, also on the basis of observed isotopic shifts, the highest frequency band was attributed to a librational mode primarily involving hindered rotation of the benzene moiety in the top-of-the-T site about one of its in-plane axes.

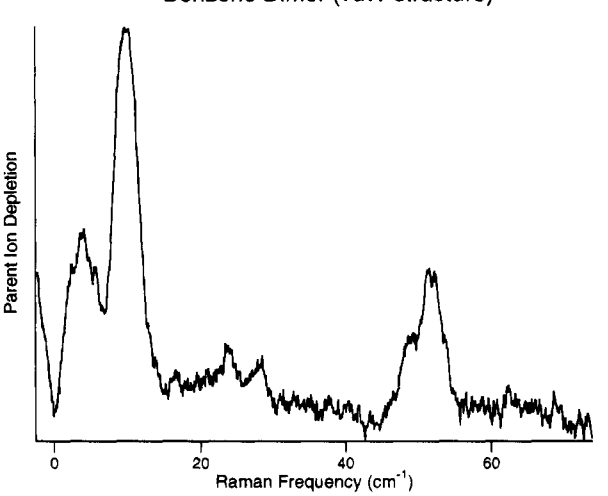

Figure 5. Mass-selective ILSRS spectrum of the fully protonated benzene dimer in the low-frequency (intermolecular vibrational) region. To obtain this spectrum ω_3 was set to the $S_1 \leftarrow S_0$ 0_0^0 band of the species.

Very recently, Maxton et al.[60] have made more sensitive mass-selective ILSRS measurements on benzene dimer than those of Venturo and Felker. Figure 5 shows a spectrum of the fully protonated species. With the increased sensitivity additional bands have been observed in the 20−30 cm^{-1} region, and the band in the 47−53 cm^{-1} region has been found to be a doublet. This additional information should help facilitate the eventual extraction of IPS parameters from the experimental results. In regard to this goal it is also clear that an increase in the resolution of the IDSRS measurements would be a very valuable advance. Such a capability is currently under development.

IV. Heterogeneous Complexes

A. Phenol–X Complexes

Hartland et al.[61] have reported an extensive mass-selective ILSRS study of intramolecular vibrational transitions in phenol−X one-to-one complexes with X being Ar, CH_4, N_2, benzene, phenol, water, ethanol, methanol, diethyl ether, or ammonia. Spectra were reported in the CC stretch (~1000 cm^{-1}), CO stretch (~1260 cm^{-1}), CH stretch (~3070 cm^{-1}), and OH stretch (3500−3660 cm^{-1}) regions. Limited results were also reported for complexes involving substituted phenols.

Figures 6 and 7 show mass-selective ILSRS spectra for a variety of phenol complexes in two regions of the vibrational spectrum. These results were (and are) useful in a number of respects. First, they clearly demonstrated that mass-selective ILSRS is applicable throughout the vibrational fundamental region at subwavenumber resolution. Second, the spectra were used to identify and characterize hydrogen-bond "marker" bands—phenolic vibrational resonances whose frequencies shift in a regular way upon hydrogen bonding. For example, the CO (Figure 6) and OH (Figure 7) stretch fundamentals of

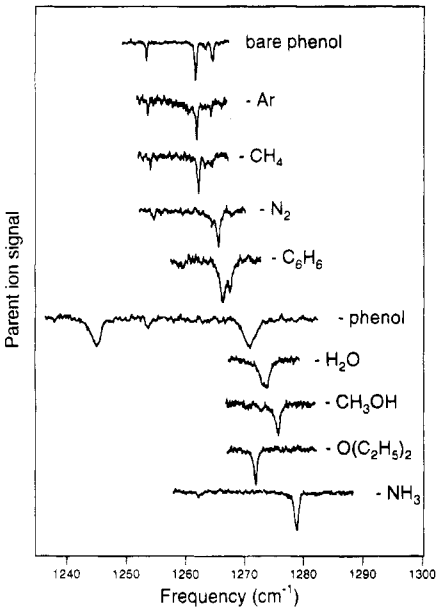

Figure 6. Mass-selective ILSRS spectra of phenol complexes in the region of the CO stretch fundamental of phenol. The strongest depletion for bare phenol (at 1261.7 cm^{-1}) was assigned to the CO stretching fundamental of the molecule. For further details see ref 61.

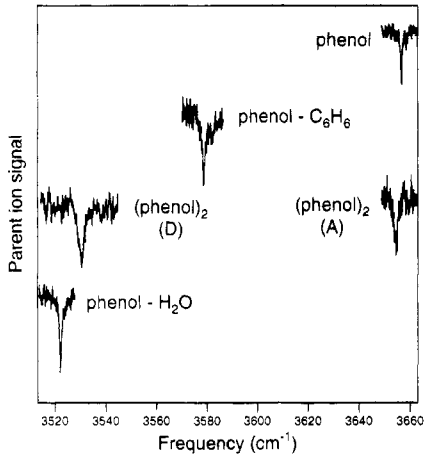

Figure 7. Mass-selective ILSRS spectra in the region of the OH stretch fundamental of phenol for bare phenol and the complexes phenol–benzene, phenol dimer, and phenol–water. In the phenol dimer spectra A refers to the hydrogen acceptor moiety and D to the hydrogen donor moiety in the hydrogen-bonded species. For further details see ref 61.

phenol shift blue and red, respectively, when phenol is the hydrogen donor in a hydrogen bond. Third, the results provide data for comparison with theoretical studies of the relevant complexes (e.g., see ref 62). Such comparisons are essential for refining the way in which intermolecular interactions are treated theoretically. Fourth, in some cases the spectroscopic results provide information with regard to the geometries of the complexes. For example, the phenol dimer results in the OH stretch region (Figure 7) strongly suggested that the dimer is such that one phenol is a hydrogen donor and the other a hydrogen acceptor (via its oxygen atom) in a dimer bound by an intermolecular hydrogen bond. This information, in conjunction with rotational spectroscopic results, has led to a structure for the dimer.[63]

Figure 8 shows spectra that pertain not to phenol-localized vibrational resonances but to resonances

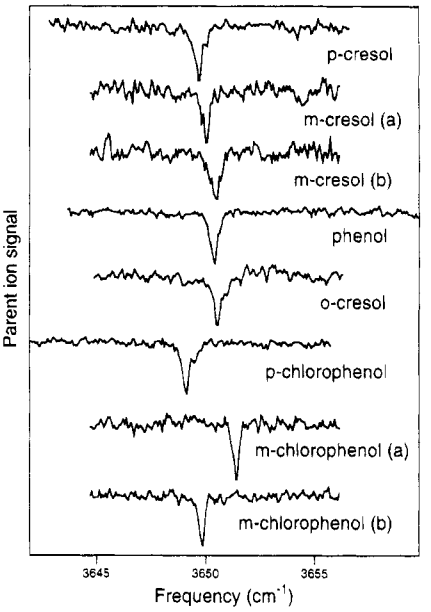

Figure 8. Mass-selective ILSRS spectra in the region of the water symmetric-stretch fundamental for phenol–water and substituted phenol–water complexes. For further details see ref 61.

localized in the water moiety of phenol–water and substituted phenol–water complexes. These spectra, and analogous ones for phenol–benzene and phenol–ammonia complexes, are examples of the capability of mass-selective ILSRS to probe the vibrational resonances of all the moieties that make up a molecular complex or cluster. Results such as these have allowed for the characterization of how solvent-localized vibrational modes shift upon hydrogen-bonding with phenolic species. For example, the data of Figure 8 indicate that the water symmetric stretch shifts a few cm^{-1} to the red when water serves as a hydrogen acceptor in a hydrogen-bonding interaction with a phenol. Similar results were found to obtain for the NH symmetric stretch of ammonia. In the case of phenol–benzene complexes, Hartland et al. found a characteristic red shift for the benzene-localized ν_1 fundamental and a characteristic blue shift for the ν_2 fundamental upon complex formation. Such results on solvent species represent data that are useful in assessing the accuracy of theoretical treatments of solute–solvent complexes.[62] Moreover, they are useful in helping one to come to a picture of the gross structural forms of the relevant complexes and others like them.

The mass-selective IDSRS study on phenol complexes also produced information on the vibrational dynamics of the species. Such information was obtained by nanosecond time-resolved IGSRS experiments and by vibrational line-width measurements. From the former Hartland et al.[61] found that all of the phenol–X complexes held together by a hydrogen bond had lifetimes considerably smaller than the laser pulsewidths (7 ns) subsequent to vibrational excitation at frequencies greater than ~1000 cm^{-1}. In contrast, the phenol–Ar and phenol–methane complexes, species in which the solvent moiety is above the phenyl ring of the phenol, were found to live for nanoseconds or longer subsequent to excitation in the 1000 cm^{-1} region. The conclusion is that vibrational energy flow is considerably faster in

hydrogen-bonded phenol complexes than in those without hydrogen bonds. Evidently the vibrational coupling of phenolic modes with hydrogen-bond vibrational modes is significantly stronger than the coupling of phenolic modes with the intermolecular vibrations of the Ar and methane complexes. (One also notes the disparity between the vibrational lifetimes of the phenol hydrogen-bonded complexes and the considerably longer lifetimes of the benzene dimer and trimer upon excitation to similar energies. See sections III.C and V.E.)

Line-width information on the vibrational dynamics of the complexes was found to be interesting in several respects. First, in phenol–water the line-width of the OH symmetric stretch fundamental was found to be a factor of about 4 narrower than the phenolic OH fundamental. This indicates a lifetime four times longer for the former vibrational level, despite it being at a higher energy. Similar mode-selective dynamics have been observed in smaller hydrogen-bonded complexes.[3] Second, line widths in the region of the CO stretch (Figure 6) indicated an enhanced relaxation of the excited CO stretch in hydrogen-bond species relative to non-hydrogen-bonded ones. This is in keeping with the time-resolved IGSRS studies of lower frequency vibrational transitions (see above). Third, the line widths of the symmetric NH stretch of the ammonia complexes indicated significantly faster relaxation of this vibration than of the analogous water vibrational mode in corresponding water complexes. With regard to this latter point, however, it was noted that one had to be wary of the contributions of inhomogeneous broadening (in particular from internal rotational levels) to the observed bandwidths.

It is pertinent to mention that other studies of the ground-state vibrational spectroscopy of phenol–X complexes have been performed apart from that of Hartland et al.[61] These include a theoretical study,[62] stimulated emission depletion experiments,[6,7] and a recent infrared–ultraviolet double resonance study.[64] There is no discrepancy between the results of these studies to the extent that they overlap one another. A comparison of the studies does, however, highlight the complementarity of the various spectroscopic approaches.

B. Benzene–X Complexes

1. Intramolecular Raman Transitions

Intramolecular vibrational transitions in numerous benzene–X complexes have been characterized by Hartland et al.[12] by using mass-selective IDSRS. One interesting aspect of these results with respect to the benzene-localized ν_1 fundamental (ring-breathing mode) is that they indicate quite long-lived ν_1-excited states for the complexes, despite the fact that such states are several hundreds of cm^{-1} above the dissociation thresholds of the species. In particular, Figure 9 shows mass-selective FT-IGSRS spectra for several such complexes measured with the REMPI probe pulse tuned to the $1_1^0 6_0^1$ vibronic band and separated by >10 ns from the Raman pump pulse. The very presence of a signal in such an experiment is proof of an excited vibrational-state lifetime on the order of nanoseconds. As with ν_1-excited benzene dimer, such lifetimes are considerably longer than one might expect given the large vibrational densities of states for these species near 1000 cm^{-1} and given an open predissociation channel. A second noteworthy aspect of the results in Figure 9 is that they are a clear demonstration of the species selectivity available with mass-selective IDSRS. All of the resonances in Figure 9 are very close in frequency to the ν_1 fundamental of benzene monomer. Further, all of the spectra correspond to samples in which the benzene molecule is the predominant species. Despite these two factors, however, one sees that the Raman spectra of the complexes can be measured to the exclusion of Raman bands from other major species in the sample. Finally, the results pertaining to the intramolecular bands of benzene–X complexes illustrate one of the principal advantages of Raman spectroscopy in studies of molecular complexes. In particular, note the simplicity of the spectra in Figure 9—single, narrow features are present in each. This behavior reflects the fact that rotational structure in a gas-phase Raman band is very often absent any appreciable P-, R-, O-, or S-branch features and is comprised instead of an overwhelmingly dominant ^qQ branch. This behavior can be very advantageous in cluster studies because it facilitates the measurement of vibrational frequencies (and hence vibrational-frequency shifts upon complexation) and the characterization of vibrational splittings.

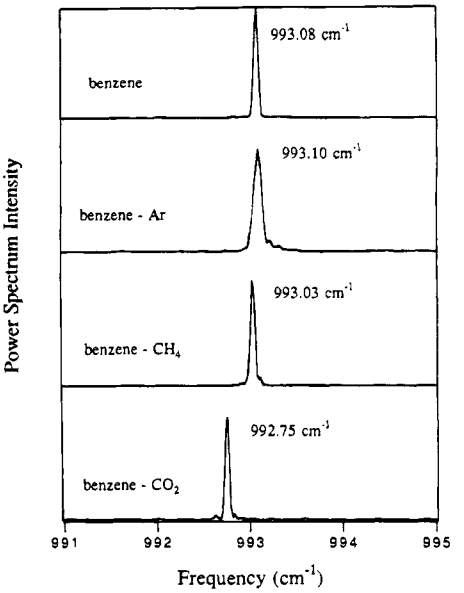

Figure 9. Fourier-transform IGSRS results pertaining to the benzene-localized ν_1 fundamental of benzene, benzene–Ar, benzene–CH_4, and benzene–CO_2. The resolution in each spectrum is 0.05 cm^{-1}, except in the benzene–Ar one, where it is 0.08 cm^{-1}. For further details see ref 12.

2. Intermolecular Raman Transitions

A mass-selective IDSRS study of intermolecular vibrational transitions in benzene–X complexes has been reported by Venturo and Felker.[65] The experiments were performed on jet-cooled benzene–Ar, –Kr, and $-N_2$ (and isotopomers thereof) at about 0.3 cm^{-1} resolution. For each of the species only a single van der Waals Raman band was observed by mass-selective ILSRS with ω_3 tuned to the 6_0^1 band of the

complex. The observed bands fall in the range between 30 and 38 cm^{-1}. They exhibit broad rotational band contours, are absent a ^qQ branch, and have polarization ratios close to 0.75. Perdeuteration of the benzene moiety shifts the bands to the red by 5−10%. By tuning ω_3 2−3 cm^{-1} to the red of the 6_0^1 vibronic band, IGSRS signals were also observed for the Raman bands, indicating that the S_0 Raman intervals correlate with somewhat smaller S_1 van der Waals intervals.

The observed Raman bands were assigned to the intermolecular bend fundamental of the complexes. The bend vibration in benzene−X species involves the movement of the X moiety parallel to the plane of the benzene with a concomitant libration of the benzene about the in-plane axis of that moiety that is perpendicular to the motion of X. The bend is doubly degenerate and nontotally symmetric in the C_{6v} benzene−Ar and −Kr complexes,[66] and the only other intermolecular mode in these species is the totally symmetric stretch. By virtue of their band contours and polarization ratios, the assignment of the observed Raman bands to non-totally symmetric transitions, and hence to ones involving the bend, was straightforward. Such an assignment is bolstered by the perdeuteration shifts (much too large for the stretch) and by the absolute frequencies of the bands (too small for the stretch). The difficult question was whether the bands were due to bend fundamentals or bend overtones. Previous work pointed to the overtone assignment.[67,68] However, Venturo and Felker chose the fundamental on the basis of three criteria: (1) a band in the vibronic spectrum of benzene−Ar, corresponding to an S_1 van der Waals interval of 31 cm^{-1}, had been firmly assigned to the excited-state bend fundamental from analysis of its resolved rotational structure,[69] (2) full three-dimensional quantum calculations employing the latest *ab initio* derived intermolecular potential for benzene−Ar had found the bend fundamental to be near 30 cm^{-1},[70,71] and (3) the Raman results showed no hint of bands in the 15−19 cm^{-1} region, indicating that if the observed bands were overtones, their corresponding fundamentals had very little Raman intensity, an unlikely situation.

A final issue addressed by Venturo and Felker[65] was the source of the Raman intensity for the observed bands. They speculated that the Raman strength might arise from the permanent polarizability anisotropy of the benzene moiety together with the librational motion[72] of the benzene during the course of the bend. In this picture the Raman activity of the bend derives, in effect, from the rotational Raman strength of benzene molecule. In fact, subsequent calculations[73] have revealed that by this mechanism one would expect the van der Waals bend fundamental in benzene−X species to be at least as strong as the *strongest* vibrational fundamentals in the Raman spectrum of benzene. Hence, the mechanism appears to be a good description of the singular Raman strength of the bend in the van der Waals spectra of these complexes.

C. Other Aromatic−X Complexes

One expects most aromatic molecules to have appreciable in-plane vs out-of-plane permanent polarizability anisotropies like that characterizing benzene.[59] As such, one would expect the intermolecular bends of most aromatic−X complexes to have significant Raman activity like that exhibited by benzene−X complexes. Maxton et al.[73] have investigated this issue by using mass-selective ILSRS to measure Raman spectra in the 0−100 cm^{-1} region of several aromatic−X complexes, including fluorobenzene−Ar and −Kr, and fluorene−Ar and −Kr. In all of these complexes there are two nondegenerate intermolecular bends and one intermolecular stretch vibration. All of the observed spectra are consistent with both of the bend fundamentals for a given species being strongly Raman active. (Figure 10 gives examples of ILSRS and IGSRS spectra for fluorobenzene−Ar.) No evidence is found, however, for Raman bands associated with the intermolecular stretch. Hence, the results are consistent with a general picture in which the strongest intermolecular Raman bands are those associated with a vibration that entails (at least in part) the libration (or rotation) of moieties having large permanent polarizability anisotropies. In addition, the results indicate that reasonably good values for the frequencies of aromatic−X bend fundamentals can be calculated by assuming that changes in inertial parameters[72] (rather than changes in potential-energy surfaces) are the dominant factors affecting the frequencies. Finally, the results represent another example of how Raman-based spectroscopies can provide information on vibrational transitions that are not readily accessible to other spectroscopic methods.

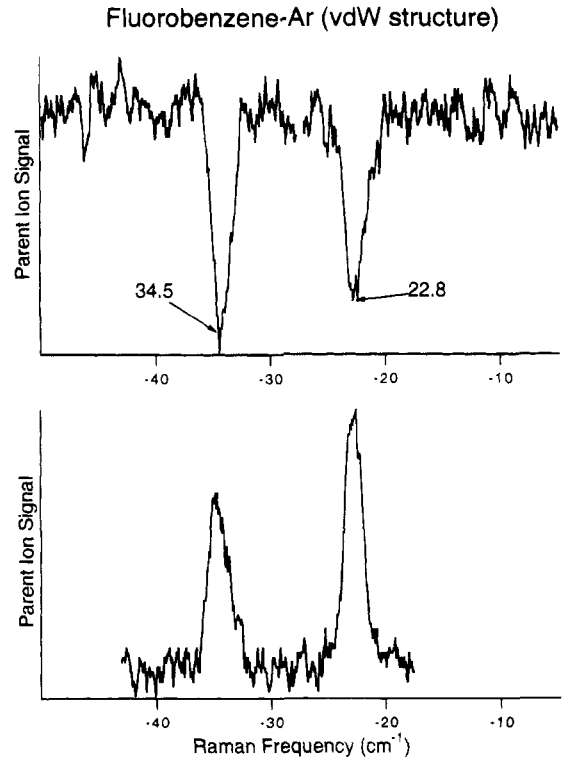

Figure 10. (Top) Mass-selective ILSRS spectrum of fluorobenzene−Ar taken in the intermolecular vibration region. To obtain these results ω_3 was tuned to the $S_1 \leftarrow S_0$ 0_0^0 band of the complex. (Bottom) Mass-selective IGSRS spectrum of fluorobenzene−Ar in the intermolecular vibration region. To obtain these results ω_3 was tuned slightly to the red of the 0_0^0 band.

V. Large Homogeneous Clusters

A. Nitrogen Clusters

Beck et al.[22,74] have used SRL to investigate the properties of large (>35 000 units) $(N_2)_n$ clusters formed in free-jet expansions. The experiments pertained to the spectral region of the intramolecular NN stretch fundamental near 2330 cm^{-1} and were performed at 90 MHz resolution. The major focus was on characterizing the clusters as a function of the distance downstream from the expansion orifice. In this regard, the high spatial and spectral resolution available to the SRL method proved invaluable. The following briefly summarizes their observations for a pure N_2 expansion. At the very smallest reduced distances—$X/D = 0.2$, where X is the distance from the orifice and D is the nozzle diameter—only Q-branch features due to N_2 monomer were observed. At $X/D = 1.2$, however, a polarized band several tenths of a cm^{-1} wide and shifted by about 3.5 cm^{-1} to the red of the monomer fundamental frequency was observed. The onset of this feature was found to coincide with visibly apparent scattering of the laser beams by the molecular beam, consistent with the formation of large clusters in this part of the expansion. For larger X/D values, up to about $X/D = 21$, this band shifted steadily to the red. At $X/D = 21$, however, the onset of a second band several tenths of a cm^{-1} to the blue was observed. This band grew in intensity relative to the first (which vanished at $X/D = 33$) and shifted to the blue as X/D was increased from 21 up to the Mach disk of the expansion at $X/D \simeq 100$.

By comparison of their molecular-beam results with SRL spectra measured for condensed-phase samples of N_2 as a function of temperature, Beck et al.[22] were able to address several important issues with regard to the formation and properties of the nitrogen aggregates. First, a very convincing case was made for assigning the first-observed aggregate band to liquid clusters and the second, blue-shifted one to clusters frozen in the β-crystalline phase of bulk N_2. Both the absolute band positions and their shifts with increasing X/D (i.e., decreasing temperature) could be perfectly correlated with the condensed-phase observations by making these assignments. Thus, their results pointed to the direct observation of a cluster phase change and cluster phase coexistence in the molecular beam. Second, they were able to assign temperatures to the clusters at the various X/D values by using the observed band positions as a thermometer. As a result they could show that the cluster temperatures were significantly larger than the monomer rotational temperatures (as determined by the intensity pattern of the Q-branch) at any given point in the expansion. This effect they attributed to the heat of condensation released to the internal modes of the clusters and to the lack of thermodynamic equilibrium between aggregates and the monomer species in the expansion. From their bandshift–temperature correlation they were also able to show that the liquid N_2 clusters at $X/D > 7.5$ in the expansion were supercooled below the triple point of N_2, the point at which freezing to the β solid occurs in an equilibrium, bulk sample. The lack of bulk SRL spectra corresponding to supercooled N_2 samples prohibited them, however, from being able to assign precise temperatures to the liquid clusters in the supercooled regime. Third, they used their data to assess two competing models of the freezing process in the expansion—the adiabatic (or sudden) model and the isothermal (or gradual) model. By assuming the isothermal model, which implies liquid–solid phase coexistence within a cluster, they estimated the rate of cluster freezing by comparing the integrated intensities of the liquid and solid Raman bands as a function of X/D. With this rate they could estimate the rate of heat release due to condensation. Accounting also for evaporative cooling of the clusters, they then calculated cluster temperatures as a function of X/D. These calculated curves were found to be qualitatively different than those derived from the data for the solid clusters. In short, they ruled out the isothermal model and found the observed behavior to be more consistent with adiabatic freezing. Assuming the latter to obtain, they calculated a value of 34 K for the degree of supercooling of the liquid by using (a) the experimentally derived temperature of the first solid clusters to appear, (b) knowledge of the heat of fusion, and (c) extrapolated values for the heat capacities of liquid and solid N_2. This value, they pointed out, represents a lower limit to the temperature of the supercooled clusters, given that the actual freezing process probably lies somewhere intermediate between the adiabatic and isothermal limits. Finally, the SRL data on pure N_2 expansions were interpreted in terms of finite-size effects. Specifically, the observed band-shape asymmetries observed for small X/D values (and absent in condensed-phase samples) were attributed to the presence of a significant fraction of surface N_2 molecules in the clusters. The interpretation is reasonable in the light of the direction of the asymmetry (biased toward the monomer vibrational frequency) and the relatively small sizes of the clusters early in the expansion.

Besides their primary results relating to pure N_2 expansions, Beck et al.[22] also reported data pertaining to N_2 clusters in 10% N_2 in He. A striking increase in cooling rate was found for this expansion with freezing to the β solid complete by $X/D = 4$. At slightly higher X/D values (5.0) they observed rather broader bands in the gap between the spectral regions of the β- and α-type condensed-phase solids. They interpreted this behavior as being due to conversion of clusters from the β phase to a glassy phase or a disordered α-solid phase. At still higher X/D (=6.0) the measured spectrum indicated a more ordered α solid at a temperature of about 33 K, suggesting a partial annealing of the disordered clusters present at $X/D = 5.0$. These results provide an example of the difference between condensation dynamics in a seeded monoatomic expansion vs that in a pure diatomic one.

Following the study by Beck et al., Barth et al.[75] reported the results of CRS experiments on jet-cooled N_2 aggregates at a resolution of about 0.2 cm^{-1}. At a fixed distance from the expansion orifice, they measured CARS spectra in the N–N stretch region of a 10% N_2 in He expansion as a function of total stagnation pressure. With increasing pressure they observed the onset of a band at 2326.6 cm^{-1}. This

band increased in intensity with pressure such that it eventually came to dominate the Q-branch feature associated with isolated N_2 molecules. A second, weak band at 2327.6 cm^{-1} was also observed at higher expansion pressures. The results are consistent with those of Beck et al.,[22] with the redder band being due to β-solid clusters and the weak 2327.6 cm^{-1} band probably due to α-solid clusters. By correlating these vibrational CARS measurements with CSRS spectra measured in the <100 cm^{-1} region, Barth et al. suggested that the β-solid clusters underwent supercooling prior to converting to the α phase. Their reasoning rested on the assumption that cluster temperature was not too far different than the rotational temperature of monomeric N_2 for any given expansion conditions. However, a direct measure of cluster temperatures, as made by Beck et al.,[22] was not possible because of insufficient spectral resolution. Hence, the question of β-phase supercooling under their expansion conditions is not entirely a settled one. In addition to observing the manifestations of N_2 aggregates in the N−N stretch region, Barth et al. also searched for the low-frequency intermolecular Raman transitions to be expected for such species. No prominent features of this sort could be observed, even under expansion conditions known to produce significant clustering. They interpreted this absence as being due to the predominant presence of clusters in the orientationally disordered β phase rather than in the α phase, consistent with the observations made in the NN stretch region.

B. CO_2 Clusters

In conjunction with their study of CO_2 dimer Pubanz et al.[30] observed a spectral feature that could be attributed to aggregates of CO_2. The feature was observed in the CARS spectra of CO_2/He expansions in the region of the lower frequency member of the $2\nu_2-\nu_1$ Fermi dyad. The band occurs in the same spectral range as that of the analogous band in solid CO_2 and was found to shift farther from the Q branch of CO_2 monomer as its fractional intensity increased. Subsequent work by the Nibler group[11] used folded BOXCARS to measure spectra of intermolecular transitions in CO_2 clusters. Their initial results revealed the presence of a cluster band near 70 cm^{-1}. The implication of this early nonlinear Raman work on CO_2 clusters was to point to the prominent existence of solidlike species under the expansion conditions employed.

The next advance in the study of CO_2 clusters was reported by Barth and Huisken.[19] They employed CSRS with a folded BOXCARS geometry to measure low-frequency spectra of 10% CO_2 in He expansions. They observed bands—one near 70 cm^{-1} and the other near 90 cm^{-1}—that could be attributed to the E_g and T_g- librational bands, respectively, of crystalline CO_2 clusters. The characteristics of these bands were observed to change with increasing distance from the expansion orifice. In particular, both bands shifted to the blue and decreased in width with increasing *X/D*. This behavior was compared with the temperature dependence observed for the analogous bands in bulk CO_2(s).[76] The similarity between the cluster and bulk phase trends strongly suggested that the evolution of the cluster bands could be attributed to a decrease in temperature as *X/D* increased. On the basis of the correlation with the results in the bulk the authors were able to assign a temperature to the clusters at the different *X/D* values. These cluster temperatures were compared with CO_2 monomer rotational temperatures derived from the relative intensities of rotational Raman transitions present in the same spectra. The two sets of temperatures (monomer and cluster) were found to track each other very well, suggesting near-equilibrium between the monomers' rotational and the clusters' librational degrees of freedom. This result provides an interesting contrast to the pronounced nonequilibrium between monomer and cluster modes found by Beck et al.[22] for N_2 clusters in pure N_2 expansions (see above). One point of difference between the cluster librational bands reported in ref 19 and those observed for the bulk crystal is that the former are significantly broader than the latter. This difference was attributed to contributions to the cluster spectra from species of different sizes and, possibly, different temperatures.

Recent CARS results by Lee et al.[20] further extend the characterization of crystalline CO_2 clusters. Specifically, the group has reported the observation of an A_g-T_g factor-group splitting in the lower member of the $2\nu_2-\nu_1$ Fermi dyad of clusters formed in expansions of 5% CO_2 in He. The reported spectrum matches the spectra of equilibrium solid samples very well with regard to line positions and relative intensities of the two factor-group components. Hence, it provides additional strong evidence for the presence of long-range order in the clusters. In addition, cluster temperatures were derived by two independent correlations of cluster spectral parameters with those of the equilibrium bulk solid. Namely, both band-position and factor-group-splitting correlations were made and were found to yield cluster temperatures that agreed with one another to within experimental error (±5 K). In contrast, the widths of the cluster bands were found to be about 2 times larger than those for bulk samples at the corresponding temperatures. This was attributed primarily to cluster-size variations within the molecular-beam volume sampled in the experiment, although the possible influences of temperature variations and crystal defects were also noted. Finally, Lee et al. also reported a CARS spectrum corresponding to the phonon region of the clusters. As in ref 19 both the E_g and T_g librational components were observed. The presence of these bands would, of course, be expected for crystalline CO_2 aggregates.

C. C_2H_2 Clusters

In their CARS study of factor-group splittings in CO_2 clusters Lee et al.[20] also reported similar results for clusters of a second species known to crystallize in a face-centered-cubic lattice—acetylene. The experiments were performed on a neat C_2H_2 expansion and pertained to the region of the C−C stretching mode of the molecule. As with CO_2, two bands were observed that matched in position and relative intensity the A_g and T_g factor-group components observed for the face-centered-cubic equilibrium solid.

This behavior was interpreted as arising from nanocrystals of acetylene. The absolute band positions and the factor-group splittings in the cluster spectrum were used to obtain two independent temperature measurements of the clusters by comparison to the spectra of bulk crystalline samples. The temperatures so obtained were the same to within experimental error (±10 K) and gave a value of 150 K for the particular expansion conditions and *X/D* value employed.

D. Ammonia Clusters

Barth and Huisken[77] have reported a CARS study of NH_3 clusters in the spectral region from 3000 to 3600 cm^{-1}. This region contains the symmetric stretch fundamental (ν_1), the asymmetric stretch fundamental (ν_3), and the first overtone of the degenerate bend ($2\nu_4$) of ammonia. With expansion conditions changing so as to increase cooling, these researchers observed spectra that evolved from containing only ammonia monomer features to ones containing prominent, red-shifted, broad bands. The latter bands, which match the positions of the ν_1, ν_3, and $2\nu_4$ bands observed for condensed-phase ammonia, were assigned to ammonia clusters. Mass-spectrometric analysis of the molecular-beam samples indicated that the clusters producing the CARS signals were likely to be comprised of 5–50 NH_3 moieties. In addition to the broad, red-shifted cluster features observed in the CARS spectra, a narrow band shifted slightly (3.5 cm^{-1}) to the red of the monomer's ν_1 Q-branch also grew in as expansions became colder. It was suggested that this feature might correspond to the ν_1 band of smaller clusters (i.e., dimer, trimer) and/or that it might arise from the ν_1 fundamentals of ammonia moieties residing on the surface of larger clusters (i.e., moieties whose H atoms do not participate in intermolecular bonding). The latter possibility is an intriguing one in that it would allow for the ready probing of the properties (e.g., dynamical characteristics) of surface vs interior moieties in ammonia clusters. Nevertheless, a definitive assignment for the narrow band must await further spectroscopic studies.

E. Benzene Clusters

1. Intramolecular Raman Transitions

Henson et al.[29] have reported mass-selective IDSRS results on jet-cooled benzene trimer and higher clusters. The data pertain to the ν_1 and ν_2 spectral regions. The most extensive results are for the trimer. For that species there are several key observations. The first is that for the fully protonated and fully deuterated isotopomers there is only one band in the ν_1 and one in the ν_2 spectral regions, respectively. Second, for the two mixed isotopomers studied—$(h_6)_2$–d_6 and h_6–$(d_6)_2$—there is only a single h_6-localized and a single d_6-localized ν_1 band, and similarly for ν_2. Third, IGSRS probe spectra, measured in the $S_1 \leftarrow S_0$ $1_1^0 6_0^1$ region subsequent to excitation of the ν_1 Raman, band show structure that matches all of the 6_0^1 structure of the vibrationally unexcited trimer. Finally, the IGSRS signal from ν_1-excited levels (referred to above) was obtained with the ω_3 probe pulse delayed by about 10 ns from the stimulated Raman pump pulse. These results on the trimer led to two principal conclusions. The first is that the species is composed of symmetrically equivalent benzene moieties. This interpretation derives from the first three sets of observations enumerated above. It is also consistent with the observed trends in Raman intensities and in ν_1 and ν_2 band positions as a function of isotopic substitution. Finally, it is supported by others' experimental[78] and theoretical results.[79] The second conclusion is that the ν_1-excited trimer lives for a nanosecond or longer subsequent to ν_1 excitation. This conclusion is based on the fourth observation listed above. It is a result that fits with the abnormally slow vibrational relaxation rates of other benzene complexes excited to the ν_1 region (benzene dimer, benzene–X complexes). Nevertheless, it is one that is surprising in the light of the much faster relaxation rates to be expected for a species of this size at this vibrational energy.

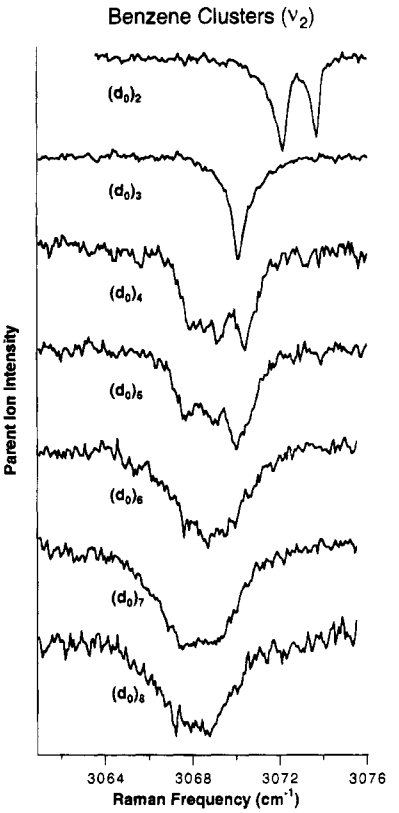

Figure 11. Mass-selective ILSRS spectra of fully protonated benzene dimer (top) through octamer (bottom) in the region of the ν_2 fundamental of benzene. The spectra were obtained by probing though the 0_0^0 band of each species and detecting the pertinent parent–ion mass. In each the resolution is about 0.3 cm^{-1}. For further details see ref 29.

For benzene clusters larger than the trimer results were reported for the fully protonated and fully deuterated species up to benzene octamer.[29] Figure 11 shows mass-selective ILSRS spectra in the ν_2 region for the fully protonated species. The principal point noted about these spectra, and that which characterizes the other results reported for the higher clusters, is that partially resolved structure is present for all the species larger than the trimer. This behavior was taken to be evidence for the presence of inequivalent benzene sites in the larger clusters, although it was noted that other interpretations, such

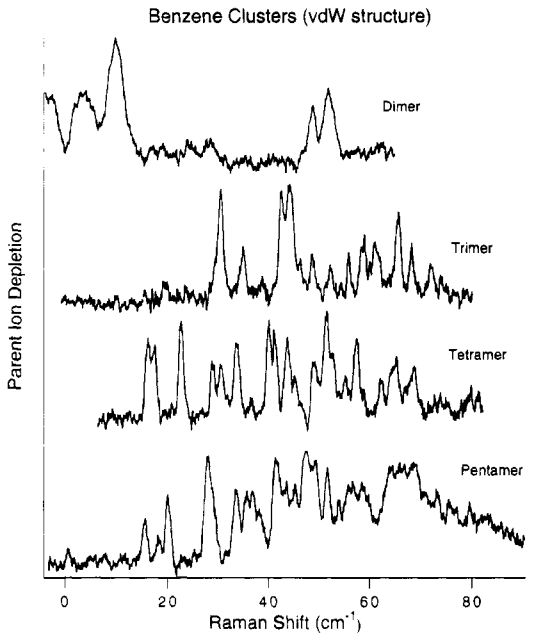

Figure 12. Mass-selective ILSRS spectra of the fully protonated dimer, trimer, tetramer, and pentamer of benzene. The spectra were obtained by setting ω_3 to the $S_1 \leftarrow S_0$ 0_0^0 bands (see ref 81) of the pertinent species.

as multiple cluster isomers, might also be valid. It is clear that results similar to those of Figure 11 but on more isotopomers and at higher spectral resolution would be a considerable aid in helping to characterize the changing nature of benzene clusters with size.

2. Intermolecular Raman Transitions

Very recently, Schaeffer et al.[80] have measured mass-selective ILSRS spectra of benzene trimer, tetramer, and pentamer from 0 to 80 cm^{-1} at about 0.2 cm^{-1} resolution. The spectra were obtained with ω_3 tuned to the $S_1 \leftarrow S_0$ 0_0^0 bands.[81] Figure 12 shows the spectra of the perprotonated trimer, tetramer, and pentamer along with the spectrum of the perprotonated dimer. These results demonstrate that there is potentially a great deal of information about intermolecular interactions to be gained from cluster-size-specific IDSRS studies of intermolecular vibrational transitions. First, it is now clear that in a given cluster many such transitions may be strongly Raman active. (For example, numerous features present in the spectra of Figure 12 represent ILSRS depletions of greater than 10%.) Second, the spectra are entirely consistent with the notion that such activity derives from the librational motions of moieties having appreciable, permanent polarizability anisotropies. (For example, virtually all of the bands in Figure 12 gain their intensity from modulation of the anisotropic part of the cluster's polarizability tensor.) This holds out the hope that the Raman intensities of intermolecular bands may be readily modeled if one knows (1) the polarizability tensors of the monomer moieties that make up a cluster and (2) the intermolecular vibrational wave functions. Conversely, and from a more practical perspective, the intensities, as well as the frequencies, of intermolecular Raman bands appear to represent a very useful measure by which to evaluate and refine intermolecular potential energy surfaces. Third, Figure 12 shows that there can be very pronounced size effects on cluster intermolecular Raman spectra. From such size effects one may expect to gain important qualitative knowledge relating to the pertinent clusters. (For example, the lack of any appreciable bands below 30 cm^{-1} in the trimer spectrum, in contrast to the presence of strong bands below 20 cm^{-1} in the dimer and the tetramer spectra, suggests that the former species does not have the loose librational modes that are present in the latter species.) Finally, it is pertinent to reemphasize the value of the broad spectral range and the species specificity available to mass-selective IDSRS in studies such as that represented by Figure 12. The former allows for the straightforward and rapid survey of the entire intermolecular spectrum of a cluster. The latter greatly facilitates the assignment of observed bands to the species from which they arise. Both will prove to be very important as one tries to characterize the size dependence of collective motions in molecular clusters.

VI. Heterogeneous Clusters

A. Ethene–Ar_n Clusters

The first observation of jet-cooled molecular clusters by a nonlinear Raman method was made by König et al.[82] in CARS experiments on ethene–Ar expansions. The CARS spectra were measured in the region of the C–C stretch fundamental of ethene near 1623 cm^{-1} at 1.1 cm^{-1} resolution. A band several cm^{-1} wide was observed to grow in about 5 cm^{-1} to the red of the Q-branch of bare ethene as the preexpansion partial pressure of Ar was varied from 2.2 to 4.9 atm, the pressure of ethene being held fixed at 0.27 atm and *X/D* being held at 7. The band was attributed to clusters of the form $(C_2H_4)_nAr_m$ with m and n between 100 and 1000. No more precise characterization of the nature of the species was possible from the data. The principal value of this early report was to show that studies of jet-cooled clusters by CARS are feasible and to suggest that such studies could be very enlightening in regard to cluster formation kinetics, given the high spatial resolution available with CARS.

B. Carbazole–Ar_n Clusters

Carbazole–Ar_n species represent a cluster system that has been extensively studied with mass-selective REMPI spectroscopy and by various theoretical approaches.[83] The size-selective vibrational spectroscopy of these species for $n = 0-14$ has been reported by Venturo et al.[84] and Henson et al.[85] both of whom employed mass-selective ILSRS. The spectra were measured in several regions at 0.15 cm^{-1} resolution on samples of carbazole seeded in pulsed expansions of 50% Ar in He. The results corresponding to the region from 1305 to 1325 cm^{-1} are shown in Figure 13.[84] Other spectra were measured near 1290 cm^{-1},[86] between 1640 and 1655 cm^{-1},[85] and in the C–H stretch region.[86] These results represent some of the first, size-selective ground-state vibrational measurements on neutral clusters of this size.

The principal value of these experiments was to demonstrate clearly the applicability of mass-selec-

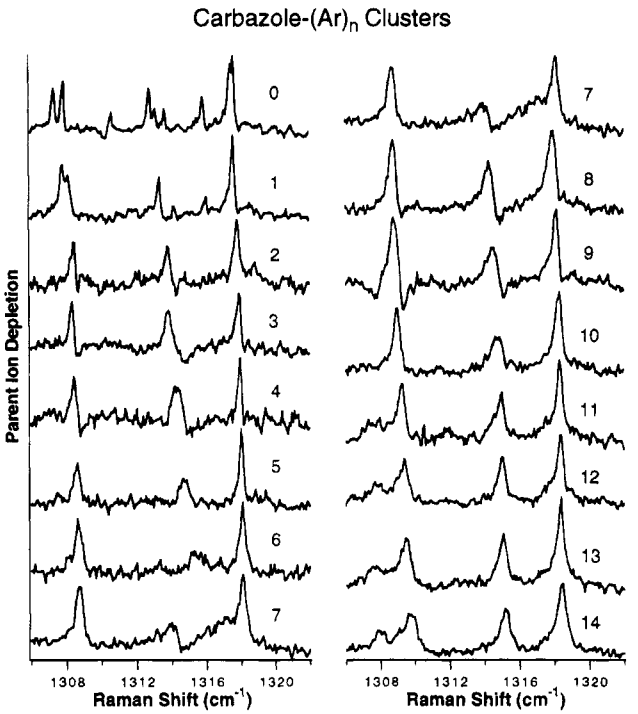

Figure 13. Mass-selective ILSRS spectra of carbazole–Ar_n clusters. The particular value of n pertaining to each spectrum is given in the figure. The spectra are plotted such that increasing ion depletion is in the positive ordinate direction. The background ion signal levels have been removed from the spectra. For further details see ref 84.

tive ILSRS to the study of larger clusters. Prior to this study it was not obvious that ILSRS signals would be observable for species having broad, relatively size-insensitive vibronic bands. For such species one expects the changes in vibronic spectra to be minimal subsequent to Raman excitation due to rapid dissipation of the vibrational energy throughout the many degrees of freedom in the cluster. Hence, one cannot rely on vibronic spectral changes to produce Raman-dependent depletions in a REMPI signal. The carbazole–Ar_n results show that such spectral changes are not necessary for a *mass-selective* ILSRS depletion to be observed. This is because Raman-dependent depletions in mass-selective REMPI signals can occur via the Raman-enhanced *fragmentation* of the neutral clusters or the cluster ions.[87] In the former case, the vibrational energy deposited in a cluster causes predissociation (evaporation) of that cluster prior to photoionization. In the latter case, the internal energy of clusters that have been photoionized after Raman excitation is greater than that of cluster ions formed by photoionization of vibrationally unexcited clusters, leading to greater post-ionization fragmentation of the Raman-excited species. In both cases, the processes produce a Raman-dependent depletion of the signal at the relevant parent–ion mass and, thus, produce a signal in mass-selective ILSRS. The existence of these depletion channels makes it possible to use mass-selective ILSRS to study clusters having more than 10 moieties (as in Figure 13) or, indeed, more than 20 or 30 moieties (as discussed in the sections below).

Aside from demonstrating some of the capabilities of mass-selective ILSRS the carbazole–Ar_n results have several other noteworthy aspects. First, in Figure 13 and in all spectral regions studied the spectra exhibit a noticeable simplification in going from bare carbazole to solvated carbazole. Vibrational "fine" structure, present for the bare molecule and presumably due to Fermi resonance interactions, gets washed out with the addition of just a few solvent species. This behavior seems to indicate that solvation somehow dilutes the strength of vibrational couplings localized within the carbazole moiety. Second, consistent with others' results[88] pertaining to vibrational relaxation rates in aromatic-doped rare-gas clusters, the widths of bands in the carbazole–Ar_n ILSRS spectra indicate relatively long-lived vibrationally excited species. For example, the 1319 cm^{-1} band of carbazole–Ar_{11} in Figure 13 has a width implying a lifetime of at least 15 ps, much longer than might be expected given the very large vibrational density-of-states for the species at this energy. Third, some of the spectra of Figure 13 exhibit negative depletions (i.e., ion gain) and/or dispersion-like band shapes. This behavior was attributed by Venturo et al.[84] to Raman-induced fragmentation effects wherein the fragmentation of Raman-excited carbazole–Ar_n clusters contributes to the carbazole–Ar_m^+ ($m < n$) photoion signal. Such behavior indicates a limitation of mass-selective ILSRS in studies of larger clusters (i.e., the possibility of undesirable spectral interference) as well as additional opportunities therein (i.e., a means by which to study ground-state evaporation processes in a size-selective way). Finally, the ILSRS results are interesting in the light of the extensive size-selective vibronic spectroscopy performed by Leutwyler and Bösiger[83] on carbazole–Ar_n clusters. In particular, the Raman spectra evolve with size in a qualitatively different way than do the vibronic spectra, demonstrating the point that vibrational resonances respond to cluster structure and dynamics differently than vibronic resonances do. Notwithstanding this, however, there are size-dependent changes in the vibrational spectra that correlate with changes in the vibronic spectra. The point is that the two sets of spectra may be expected to complement one another with regard to the information that they provide about the size evolution of cluster properties.

C. Benzene–Ar_n Clusters

The benzene–Ar_n system of clusters represents another cluster series that has been characterized extensively with size-selective vibronic spectroscopy and theoretical simulations.[89-95] In an effort to address some of the issues raised by these studies regarding structure and dynamics as a function of size Venturo et al.[96] undertook a mass-selective ILSRS study of the species for $n = 1-22$. The results pertain to the benzene-localized ν_1 and ν_2 fundamentals and were obtained at 0.15 cm^{-1} resolution. Figure 14 shows the size dependence of spectra measured in the ν_1 region. Each spectrum was obtained with the REMPI probe field tuned to the most intense feature (for that size) occurring in the region of the $S_1 \leftarrow S_0$ 6_0^1 benzene-localized vibronic band.[89] One notes several points about these spectra. First, for $n < 16$ the spectra consist of a single band (within the resolution) that shifts monotonically to the blue with increasing size. Second, between $n = 16$ and $n = 21$ the spectra consist of a resolvable

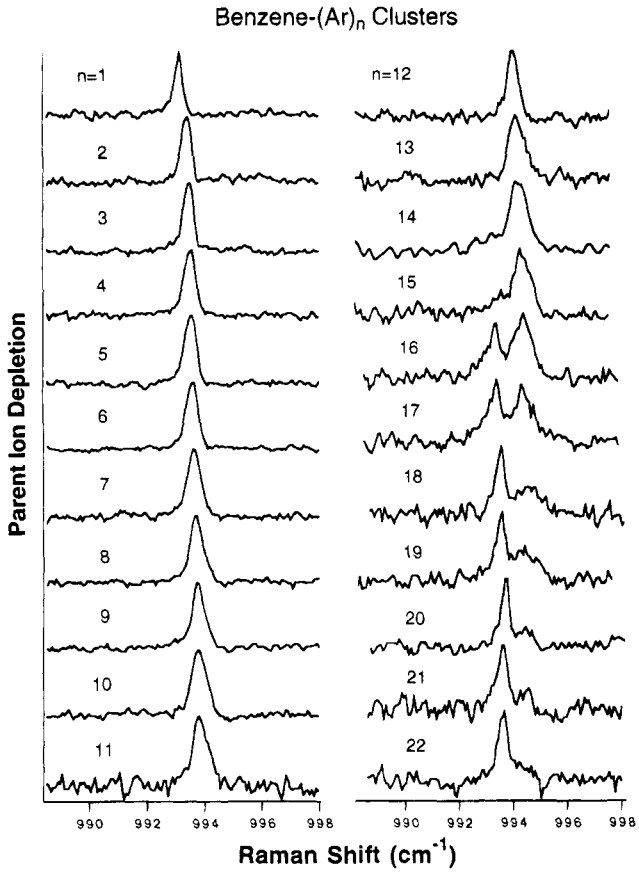

Figure 14. Mass-selective ILSRS spectra of benzene–Ar_n clusters in the region of the benzene-localized ν_1 fundamental. The number that labels each spectrum corresponds to the number of Ar atoms in the detected benzene–Ar_n^+ ion. The spectra are plotted such that the positive ordinate direction corresponds to increasing depletion. For further details see ref 96.

doublet. Third, one of the doublet bands fits in with the spectral trend established by the smaller clusters. The other one does not. Finally, the former band decreases in relative intensity in going from $n = 16$ to 21 while the latter band's intensity increases. Qualitatively similar behavior was also observed for the spectra measured in the ν_2 region near 3070 cm^{-1}. In addition to these results, mass-selective ILSRS spectra were also reported for several cluster sizes for different ω_3 (the REMPI probe frequency) values. For $n = 18$, in both the ν_1 and ν_2 spectral regions, the ILSRS spectra were found to vary appreciably depending on ω_3. Indeed, a third Raman band was found when ω_3 was tuned to the reddest vibronic feature[89] in the 6_0^1 region corresponding to this cluster size. In contrast, very little in the way of spectral changes was found when ω_3 was tuned to different vibronic bands[90] of the $n = 2$, 3, and 4 clusters.

The results of ref 96 lead to three definite conclusions. The first is that in the size range from $n = 16$ to 21 at least three cluster types are present in the molecular-beam sample. This follows from the data and from the fact that the ν_1 and ν_2 benzene fundamentals are nondegenerate. The only way that multiple ν_1 (or ν_2) bands can arise for a given value of n is if multiple cluster isomers are present for that n; that is, three Raman bands imply the existence of three cluster types. The second conclusion is that the distribution of these cluster types evolves from $n = 16$ to 21. The size evolution of relative intensities in the ILSRS spectra prove this point. In particular, the cluster type that correlates spectroscopically with those at lower values of n (the one that produces the bluer member of the doublets in Figure 14) contributes less as n increases beyond 16 and effectively vanishes beyond $n = 21$. Third, the different Raman bands in the $n = 16$–21 size range correlate with different vibronic features. This conclusion derives from the dependence of the Raman spectra on the value of ω_3. (Experimental results that are much more extensive than those of ref 96 and that pertain to this issue have been obtained.[97] These results affirm the close correlation between Raman and vibronic spectral features.)

The above conclusions bear on, but do not decide the issue of most interest in regard to the benzene–Ar_n species—that is, the nature of the difference between the cluster types in the $n = 16$–21 size range. Are such differences due to the coexistence of clusters in different phases (liquid and solid) at a given size, as suggested in one interpretation[89] of the vibronic spectroscopic results? Or, can they be attributed to static, structural differences between clusters at a given n?[93-95] Venturo et al.[96] argue for the latter interpretation. In particular, they invoke a difference in the number of Ar atoms bound in the plane of the benzene moiety as that which distinguishes between the two cluster types reflected in the spectra of Figure 14. This interpretation derives, first, from atom–atom pair-potential calculations of the minimum-energy cluster structures.[89b,94] These predict that Ar binding will occur in single layers above and below the benzene plane from $n = 1$ to 14. Beyond $n = 14$ the most favorable Ar binding site is found to be in the plane of the benzene on the periphery of that moiety. Binding in a second layer above or below the benzene plane is somewhat less favorable. These calculations suggest that in a thermal distribution of clusters having $n > 14$ one might expect some species to have Ar atoms bound in the benzene plane and others at the same size to have no Ar atoms bound in such sites. Further, one would expect the fraction of species with no in-plane Ar atoms to decrease with n until they eventually vanish altogether. Thus, the calculated results are consistent with (a) a bifurcation of cluster types in the pertinent size range and (b) a change in the relative abundances of those types with increasing n. Second, the ILSRS results show that the two cluster types contributing to the spectra of Figure 14 differ with respect to the perturbation of an in-plane vibrational mode of benzene. It is certainly reasonable to attribute this to differences in the number of Ar atoms bound in the benzene plane. Third, the ILSRS results on the $n = 2$–4 clusters as a function of ω_3 show that the distribution of Ar atoms above and below the benzene plane has little effect on the ν_1 and ν_2 Raman bands of the species, again pointing to differences in in-plane binding as the distinguishing feature between the different cluster types manifested in the Raman spectra. These points led Venturo et al.[96] to assign the blue member of the Raman doublets in the 16–21 size range to clusters having no Ar atoms bound in the benzene plane and

the red member to those with in-plane Ar atoms present. The third Raman band, given its close proximity to the red member of the Raman doublets, was assigned to a second type of cluster having Ar atoms in-plane.

While Venturo et al.[96] invoke a structural reason to rationalize their ILSRS results on benzene–Ar_n clusters, they do not exclude the possibility that the different cluster types observed may, in fact, represent clusters in different phases. One should also note that somewhat different interpretations based on structure[93–95] have also been put forth with regard to the size dependence of the vibronic spectra of these clusters. Results from a full ILSRS study of these species,[97] in conjunction with direct simulations of ILSRS spectra, may well shed more light on these questions.

D. Benzene–$(N_2)_n$ Clusters

Venturo et al.[98] have reported mass-selective ILSRS results on a second type of benzene–$(solvent)_n$ cluster, one in which the solvent species is a molecule rather than an atom. In such species there is the possibility of investigating not only benzene-localized Raman transitions, but also the Raman resonances localized in the solvent moieties. One generally expects the latter to be a more informative probe of solvent structure and dynamics than the former. The clusters studied in ref 98 involved N_2 as the solvent species. The ILSRS spectra were measured in the NN stretch region near 2330 cm^{-1} at a resolution of 0.15 cm^{-1}. Spectra were reported for clusters as large as benzene–$(N_2)_{32}$. Figure 15 shows the results for $n = 1-16$, obtained by tuning ω_3 to the peak of the benzene-localized $S_1 \leftarrow S_0$ 6_0^1 vibronic structure[99,100] at the relevant cluster sizes. Several features were noted in the data. First, for $n = 1$ there is only a single band in the spectrum, shifted by 2 cm^{-1} to the red of the free N_2 molecule's vibrational frequency. Already at $n = 2$, however, a doublet is present. The red member of the doublet ("band a") is just slightly red of the $n = 1$ band. The blue member ("band b") is shifted by 1.0 cm^{-1} back toward the bare molecule frequency. Third, this doublet structure persists up to $n = 10$. However, with increasing n band b gains in intensity relative to band a and both bands shift gradually to the red. Fourth, at $n = 11$ a third band ("band c") starts to grow in at 2329.0 cm^{-1}. The relative intensity of this band increases with n until at $n \approx 19$ it is close to that of band b. At the same time, bands b and c merge until they are essentially indistinguishable at $n = 20$. Fifth, the spectra from $n = 20$ to 29 are dominated by the broad feature correlating with the merger of bands b and c and centered at 2328.0 to 2328.4 cm^{-1}. Finally, at $n = 30-32$ this broad feature starts to split up into resolvable structure.

The above results were interpreted to be the manifestations of the building up of the first N_2 solvent shell about the benzene molecule.[98] It was noted that the benzene–N_2 complex has a geometry in which the N_2 moiety is bound above the center of the benzene ring.[99,101] Hence, the band observed for the $n = 1$ species was attributed to N_2 bound in this central site. Since band a for the larger clusters correlates with the $n = 1$ band, it was also assigned

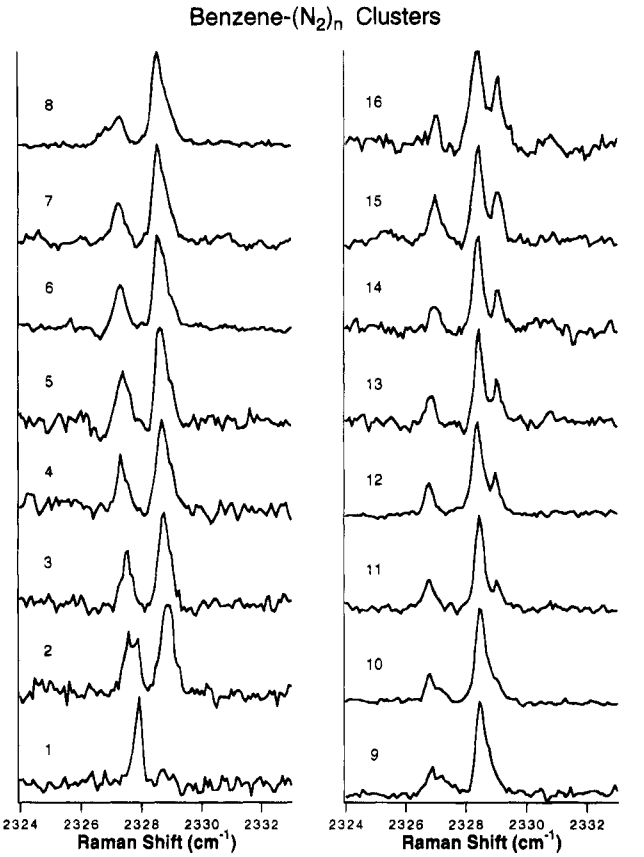

Figure 15. Mass-selective ILSRS spectra of benzene–$(N_2)_n$ clusters in the region of the NN stretch fundamental. The number that labels each spectrum corresponds to the number of N_2 moieties in the detected benzene–$(N_2)_n^+$ ion. The spectra are plotted such that the positive ordinate direction corresponds to increasing depletion. For further details see ref 98.

to the NN stretch resonances of N_2 moieties residing in central binding sites. Now, of course, there are only two central binding sites on benzene. The geometry of the $n = 1$ complex suggests that these are the most favorable binding sites for N_2. However, as soon as one of the sites is filled, different sites open up. Band b was assigned to N_2 moieties residing in this second type of binding site. It was suggested that the sites of this type most likely are ones in a circle around the centrally bound N_2 moiety (moieties) at a similar height above or below the benzene plane; binding in such sites would allow for the greatest van der Waals contact between molecules. Assuming this to be true, it is clear that there are more of this second type of site than of the two central binding sites. This can account for the steady increase in relative intensity of band b with respect to band a as n increases. Further, the shift of band b from the bare N_2 stretch frequency is smaller than that of band a. This is consistent with the former arising from N_2 species that interact less extensively with other moieties than centrally bound N_2 molecules do and, hence, is consistent with the binding site proposed to be associated with band b. The band that was observed to grow in at $n = 11$—band c—was assigned to N_2 molecules filling a third type of binding site. Again, a new type of site would be expected to become prevalent once the sites associated with bands a and b are filled, or nearly filled. Further, the increase in relative intensity of this band

with increasing n is consistent with the filling of a newly available site. Venturo et al.[98] suggested that the third site type likely corresponds to binding in the plane of the benzene and on the periphery of that moiety. This assignment was based on the spectral shift behavior of benzene-localized vibronic[99,100] and vibrational[97,98] bands in the size range from $n = 9$ to 12, both of which indicated a qualitative change in the perturbation of the benzene over this size range. Finally, the decrease in resolvable features beyond $n \simeq 20$ precluded any detailed conclusions about the solvent shell structure for these clusters. However, it was noted that the onset of a new Raman doublet at $n = 30$ suggests that mass-selective ILSRS spectra on even larger clusters might eventually yield important information about solvent-shell accretion beyond the first solvent shell.

VII. Summary and Conclusion

The material reviewed herein gives some idea of the value and promise of nonlinear Raman spectroscopies in studies of molecular complexes and clusters. It is clear that such spectroscopies have addressed, and will continue to address, important issues that are difficult or impossible to address by other means. It is also apparent that the different nonlinear Raman methods have different strengths with regard to these kinds of studies. SRL and CRS are particularly suited to the study of large homogeneous clusters. They have allowed for (1) the unprecedented characterization of condensation dynamics in free-jet expansions,[22,74,75] (2) the elucidation of cluster phases,[19,20,22,75] (3) the determination of cluster temperatures,[19,20,22] (4) the characterization of low-frequency collective modes in cluster ground states,[11,19,20] and (5) the assessment of the degree of long-range order in finite-size systems.[19,20,22,75] Mass-selective IDSRS, on the other hand, is particularly valuable in size- or species-selective studies of small-to-medium size species, be they homogeneous or heterogeneous in nature. Its strengths have allowed for or facilitated (1) the characterization of the size dependence of ground-state collective modes in small clusters,[58,60,65,73,80] (2) the elucidation of solvent-shell accretion in solute−solvent$_n$ clusters,[84,85,96−98] (3) the precise characterization of complexation-induced splittings, shifts, and widths of ground-state intramolecular vibrational resonances, results relevant to the structure and dynamics of small complexes and clusters,[12,28,29,47,61] (4) the correlation of ground-state and excited-state vibrational intervals,[58,65,73] and (5) the measurement of the vibronic spectra that arise from excited vibrational levels in the ground-state manifold.[28,29] Thus, one sees that the nonlinear Raman methods are complementary to one another, as well as being complementary to other classes of spectroscopic techniques.

The nonlinear Raman spectroscopy of molecular-beam samples is very far from being a mature field. One expects that many more studies of the type reviewed herein will be reported in the future. Of course, one also expects that there will be developments with regard to increasing the information content and extending the range of such studies. An increase in the routine spectral resolution available is one development that is obviously desirable and quite feasible. The extension of size-selective experiments to larger and larger clusters is also both desirable and feasible. Besides these developments, one expects that new classes of Raman-based experiments will soon become prevalent. A picosecond-resolved version of mass-selective IGSRS is conceivable and may well provide a widely applicable means by which to study ground-state cluster dynamics directly in the time domain. Such a method would also make possible, by means of rotational coherence spectroscopy,[102] the measurement of rotational constants associated with vibrational levels in the ground-state manifold. Application of mass-selective IDSRS to the study of laser-generated, jet-cooled species such as radicals, metal clusters, and biomolecules is another promising future direction. So is the use of stimulated Raman action spectroscopies in the study of mass-selected cluster ions. Given all this, it is reasonable to expect that nonlinear Raman methods will remain a fruitful source of ground-state spectroscopic information on jet-cooled species for many years to come.

Acknowledgments. The authors are indebted to G. V. Hartland, B. F. Henson, V. A. Venturo, and S. M. Ohline for their essential contributions to much of the work reviewed herein. Financial support for the nonlinear Raman work in P.M.F.'s laboratory has been provided by the U.S. Department of Energy, Office of Basic Energy Sciences under grant no. DE-FG03-89-ER14066. We are grateful for this support.

VIII. References

(1) Celii, F. G.; Janda, K. C. *Chem. Rev.* **1986**, *86*, 507.
(2) Nesbitt, D. J. *Chem. Rev.* **1988**, *88*, 843.
(3) Miller, R. E. *Adv. Mol. Vib. Collision Dyn.* **1991**, *1*, 83.
(4) Cohen, R. C.; Saykally, R. J. *J. Phys. Chem.* **1992**, *96*, 1024.
(5) Frye, D.; Lapierre, L.; Dai, H.-L. *J. Opt. Soc. Am. B* **1990**, *7*, 1905.
(6) Ebata, T.; Furukawa, M.; Suzuki, T.; Ito, M. *J. Opt. Soc. Am. B* **1990**, *7*, 1890.
(7) Stanley, R. J.; Castleman, A. W. *J. Chem. Phys.* **1991**, *94*, 7744.
(8) Takayanagi, M.; Hanazaki, I. *J. Opt. Soc. Am. B* **1990**, *7*, 1898.
(9) Levy, D. H. *Adv. Chem. Phys.* **1981**, *47*, 323.
(10) Ito, M. *J. Mol. Struct.* **1988**, *177*, 191.
(11) Nibler, J. W.; Yang, J. J. *Ann. Rev. Phys. Chem.* **1987**, *38*, 349.
(12) Hartland, G. V.; Henson, B. F.; Venturo, V. A.; Hertz, R. A.; Felker, P. M. *J. Opt. Soc. Am.* **1990**, *7*, 1950.
(13) Weber, P. M.; Rice, S. A. *J. Chem. Phys.* **1988**, *88*, 6107.
(14) Zhang, Q.; Kandel, S. A.; Wasserman, T. A. W.; Vaccaro, P. H. *J. Chem. Phys.* **1992**, *96*, 1640.
(15) For a review, see: Felker, P. M. In *Laser Techniques in Chemistry*; Rizzo, T. R., Myers, A. B., Eds.; John Wiley & Sons, Inc.: New York, in press.
(16) Huber-Wälchli, P.; Guthals, D. M.; Nibler, J. W. *Chem. Phys. Lett.* **1979**, *67*, 233.
(17) Duncan, M. D.; Österlin, P.; Byer, R. L. *Opt. Lett.* **1981**, *6*, 90.
(18) Eckbreth, A. C. *Appl. Phys. Lett.* **1978**, *32*, 421.
(19) Barth, H. D.; Huisken, F. *Chem. Phys. Lett.* **1990**, *169*, 198.
(20) Lee, K. H.; Brown, K. W.; Triggs, N. E.; Richardson, A. D.; Rich, N. H.; Nibler, J. W. *J. Chem. Phys.* **1993**, *98*, 10100.
(21) Owyoung, A. In *Laser Spectroscopy IV*; Walther, H., Rothe, K. W., Eds.; Springer-Verlag: Berlin, 1979.
(22) Beck, R.; Hineman, M. F.; Nibler, J. W. *J. Chem. Phys.* **1990**, *92*, 7068.
(23) Bronner, W.; Oesterlin, P.; Schellhorn, M. *Appl. Phys. B* **1984**, *34*, 11.
(24) Esherick, P.; Owyoung, A. *Chem. Phys. Lett.* **1983**, *103*, 235.
(25) Esherick, P.; Owyoung, A.; Pliva, J. *J. Chem. Phys.* **1985**, *83*, 3311.
(26) Hartland, G. V.; Henson, B. F.; Felker, P. M. *J. Chem. Phys.* **1989**, *91*, 1478.
(27) Hartland, G. V.; Joireman, P. W.; Connell, L. L.; Felker, P. M. *J. Chem. Phys.* **1992**, *96*, 179.
(28) Henson, B. F.; Hartland, G. V.; Venturo, V. A.; Felker, P. M. *J. Chem. Phys.* **1992**, *97*, 2189.
(29) Henson, B. F.; Venturo, V. A.; Hartland, G. V.; Felker, P. M. *J. Chem. Phys.* **1993**, *98*, 8361.

(30) Pubanz, G. A.; Maroncelli, M.; Nibler, J. W. *Chem. Phys. Lett.* **1985**, *120*, 313.
(31) Novick, S. E.; Davies, P. B.; Dyke, T. R.; Klemperer, W. *J. Am. Chem. Soc.* **1973**, *95*, 8547.
(32) Barton, A. E.; Chablo, A.; Howard, B. *J. Chem. Phys. Lett.* **1979**, *60*, 414.
(33) Mannik, L.; Stryland, J. C.; Welsh, H. L. *Can. J. Phys.* **1971**, *49*, 3056.
(34) Kopec, R. L. Ph.D. Thesis, Indiana University, Bloomington, 1981.
(35) Gough, T. E.; Miller, R. E.; Scoles, G. *J. Phys. Chem.* **1981**, *85*, 4041.
(36) Miller, R. E.; Watts, R. O. *Chem. Phys. Lett.* **1984**, *105*, 409.
(37) Fredin, L.; Nelander, B.; Ribbegard, G. *J. Mol. Spectrosc.* **1974**, *53*, 410.
(38) Guasti, R.; Schettino, V.; Brigot, N. *Chem. Phys.* **1978**, *34*, 391.
(39) Hashimoto, M.; Isobe, T. *Bull. Chem. Soc. Jpn.* **1974**, *47*, 40.
(40) Koide, A.; Kihara, T. *Chem. Phys.* **1974**, *5*, 34.
(41) Brigot, N.; Odiot, S.; Walmsley, S. H.; Whitten, J. L. *Chem. Phys. Lett.* **1977**, *49*, 157.
(42) Jucks, K. W.; Huang, Z. S.; Dayton, D.; Miller, R. E.; Lafferty, W. J. *J. Chem. Phys.* **1987**, *86*, 4341.
(43) Hopkins, G. A.; Maroncelli, M.; Nibler, J. W.; Dyke, T. R. *Chem. Phys. Lett.* **1985**, *114*, 97.
(44) Maroncelli, M.; Hopkins, G. A.; Nibler, J. W.; Dyke, T. R. *J. Chem. Phys.* **1985**, *83*, 2129.
(45) Jucks, K. W.; Miller, R. E. *J. Chem. Phys.* **1988**, *88*, 2196.
(46) Jucks, K. W.; Miller, R. E. *J. Chem. Phys.* **1988**, *88*, 6059.
(47) Henson, B. F.; Hartland, G. V.; Venturo, V. A.; Hertz, R. A.; Felker, P. M. *Chem. Phys. Lett.* **1991**, *176*, 91.
(48) Henson, B. F.; Hartland, G. V.; Venturo, V. A.; Felker, P. M. *J. Chem. Phys.* **1989**, *91*, 2751.
(49) Johnson, R. D.; Burdenski, S.; Hoffbauer, M. A.; Giese, C. F.; Gentry, W. R. *J. Chem. Phys.* **1986**, *84*, 2624.
(50) Hobza, P.; Selzle, H. L.; Schlag, E. W. *J. Chem. Phys.* **1990**, *93*, 5893.
(51) Cox, E. *Rev. Mod. Phys.* **1958**, *30*, 159.
(52) Janda, K. C.; Hemminger, J. C.; Winn, J. S.; Novick, S. E.; Harris, S. J.; Klemperer, W. *J. Chem. Phys.* **1975**, *63*, 1419.
(53) Hopkins, J. B.; Powers, D. E.; Smalley, R. E. *J. Phys. Chem.* **1981**, *85*, 3729.
(54) Ebata, T.; Hamakado, M.; Motiyama, S.; Morioka, Y.; Ito, M. *Chem. Phys. Lett.* **1992**, *199*, 33.
(55) Scherzer, W.; Krätzschmar, O.; Selzle, H. L.; Schlag, E. W. *Z. Naturforsch.* **1992**, *47a*, 1248.
(56) Arunan, E.; Gutowsky, H. S. *J. Chem. Phys.* **1993**, *98*, 4294.
(57) Hobza, P.; Selzle, H. L.; Schlag, E. W. *J. Phys. Chem.* **1993**, *97*, 3937.
(58) Venturo, V. A.; Felker, P. M. *J. Chem. Phys.* **1993**, *99*, 748.
(59) Battaglia, M. R.; Buckingham, A. D.; Williams, J. H. *Chem. Phys. Lett.* **1981**, *78*, 421.
(60) Maxton, P. M.; Schaeffer, M. W.; Venturo, V. A.; Felker, P. M. To be submitted.
(61) Hartland, G. V.; Henson, B. F.; Venturo, V. A.; Felker, P. M. *J. Phys. Chem.* **1992**, *96*, 1164.
(62) Schütz, M.; Bürgi, T.; Leutwyler, S.; Fischer, T. *J. Chem. Phys.* **1993**, *98*, 3763.
(63) Connell, L. L.; Ohline, S. M.; Joireman, P. W.; Corcoran, T. C.; Felker, P. M. *J. Chem. Phys.* **1992**, *96*, 2585.
(64) Tanabe, S.; Ebata, T.; Fujii, M.; Mikami, N. *Chem. Phys. Lett.* **1993**, *215*, 347.
(65) Venturo, V. A.; Felker, P. M. *J. Phys. Chem.* **1993**, *97*, 4882.
(66) Weber, Th.; Riedle, E.; Neusser, H. J.; Schlag, E. W. *Chem. Phys. Lett.* **1991**, *183*, 77.
(67) Menapace, J. A.; Bernstein, E. R. *J. Phys. Chem.* **1987**, *91*, 2533.
(68) Bieske, E. J.; Rainbird, M. W.; Atkinson, I. M.; Knight, A. E. W. *J. Chem. Phys.* **1989**, *91*, 752.
(69) Riedle, E.; van der Avoird, A. Private communication.
(70) Bludský, O.; Spirko, V.; Hrouda, V.; Hobza, P. *Chem. Phys. Lett.* **1992**, *196*, 410.
(71) van der Avoird, A. *J. Chem. Phys.* **1993**, *98*, 5327.
(72) Mons, M.; Le Calvé, J.; Piuzzi, F.; Dimicoli, I. *J. Chem. Phys.* **1990**, *92*, 2155.
(73) Maxton, P. M.; Schaeffer, M. W.; Ohline, S. M.; Kim, W.; Venturo, V. A.; Felker, P. M. Submitted for publication.
(74) Beck, R.; Nibler, J. W. *Chem. Phys. Lett.* **1988**, *148*, 271.
(75) Barth, H. D.; Huisken, F.; Iluykhin, A. A. *Appl. Phys. B* **1991**, *52*, 84.
(76) Olijnyk, H.; Däufer, H.; Jodl, H.-J.; Hochheimer, H. D. *J. Chem. Phys.* **1988**, *88*, 4204.
(77) Barth, H. D.; Huisken, F. *J. Chem. Phys.* **1987**, *87*, 2549.
(78) Krause, H.; Ernstberger, B.; Neusser, H. J. *Chem. Phys. Lett.* **1991**, *184*, 411.
(79) van der Waal, B. W. *Chem. Phys. Lett.* **1986**, *123*, 69.
(80) Schaeffer, M. W.; Maxton, P. M.; Felker, P. M. *Chem. Phys. Lett.*, in press.
(81) Börnsen, K. O.; Lin, S. H.; Selzle, H. L.; Schlag, E. W. *J. Chem. Phys.* **1989**, *90*, 1299.
(82) König, F.; Oesterlin, P.; Byer, R. L. *Chem. Phys. Lett.* **1982**, *88*, 477.
(83) Leutwyler, S.; Bösiger, J. *Chem. Rev.* **1990**, *90*, 489.
(84) Venturo, V. A.; Maxton, P. M.; Henson, B. F.; Felker, P. M. *J. Chem. Phys.* **1992**, *96*, 7855.
(85) Henson, B. F.; Hartland, G. V.; Venturo, V. A.; Maxton, P. M.; Felker, P. M. *Proc. Soc. Photo.-Opt. Instr. Eng.* **1992**, *1638*, 63.
(86) Venturo, V. A.; Felker, P. M. Unpublished results.
(87) Felker, P. M. In *Molecular Dynamics and Spectroscopy by Stimulated Emission Pumping*; Dai, H.-L., Field, R. W., Eds.; World Scientific, in press.
(88) For example: Amirav, A.; Even, U.; Jortner, J. *J. Phys. Chem.* **1982**, *86*, 3345.
(89) (a) Hahn, M. Y.; Whetten, R. L. *Phys. Rev. Lett.* **1988**, *61*, 1190. (b) Hahn, M. Y. Ph.D. Dissertation, Department of Chemistry and Biochemistry, UCLA, 1989.
(90) Schmidt, M.; Mons, M.; Le Calvé, J. *Chem. Phys. Lett.* **1991**, *177*, 371.
(91) Schmidt, M.; Mons, M.; Le Calvé, J.; Millié, P.; Cossart-Magos, C. *Chem. Phys. Lett.* **1991**, *183*, 69.
(92) Schmidt, M.; Mons, M.; Le Calvé, J. *J. Phys. Chem.* **1992**, *96*, 2404.
(93) Schmidt, M.; Le Calvé, J.; Mons, M. *J. Chem. Phys.* **1993**, *98*, 6102.
(94) (a) Fried, L. E.; Mukamel, S. *Phys. Rev. Lett.* **1991**, *66*, 2340. (b) Fried, L. E.; Mukamel, S. *J. Chem. Phys.* **1992**, *96*, 116.
(95) Adams, J. E.; Stratt, R. M. *J. Chem. Phys.* **1990**, *93*, 1358.
(96) Venturo, V. A.; Maxton, P. M.; Felker, P. M. *Chem. Phys. Lett.* **1992**, *198*, 628.
(97) (a) Venturo, V. A. Ph.D. Dissertation, Department of Chemistry and Biochemistry, UCLA, 1994. (b) Venturo, V. A.; Felker, P. M. Manuscript in preparation.
(98) Venturo, V. A.; Maxton, P. M.; Felker, P. M. *J. Phys. Chem.* **1992**, *96*, 5235.
(99) Nowak, R.; Menapace, J. A.; Bernstein, E. R. *J. Chem. Phys.* **1988**, *89*, 1309.
(100) Li, X.; Hahn, M. Y.; El-Shall, M. S.; Whetten, R. L. *J. Phys. Chem.* **1991**, *95*, 8524.
(101) Weber, Th.; Smith, A. M.; Riedle, E.; Neusser, H. J.; Schlag, E. W. *Chem. Phys. Lett.* **1990**, *175*, 79.
(102) Felker, P. M. *J. Phys. Chem.* **1992**, *96*, 7844.